Supplementary information

Energy optimisation of plant factories and greenhouses for different climatic conditions

Till Weidner, Michael Hamm, Aidong Yang

Table of Contents

1 Energy-efficient design heuristics

1.1 General description of the systems

It was assumed that the plant factory (PF) is housed in a concrete building with no material transfer and little heat loss to the environment, which means that it requires continuous dehumidification due to plant transpiration. For the greenhouses (GH), a concrete wall on the side facing away from the sun reduces the heat loss [1] and serves as a structure for the air handling unit (AHU) which is part of the heating, ventilation and air conditioning system (HVAC, SI 1.3)). To balance lighting with cooling requirements, the cover material was based on the annual solar radiation, with ethylene tetrafluoroethylene (ETFE) being chosen for cold climates (SI 1.2), otherwise Polycarbonate (PC) [2,3]. For very sunny locations, the installation of a removable refraction lens cover (RLC) [4] was assumed when it would be favourable more than three months in a year (SI 1.2), drastically reducing solar heat influx. To mitigate seasonal extremes, mild or strong seasonal whitewash (SI 1.4) was optionally applied if it would not reduce the required daily light integral (DLI) and a thermal screen (SI 1.5) would be applied at night if required [5]. Additional cooling was optional through fogging [6] and venting in the open GH (SI 1.6). Light-emitting diodes (LED) would supply the required moles of light (daily light integral, DLI) light in the PF and supplement the natural light in the GHs (SI 1.7). All three systems benefit from a LED water-cooling system [7], which enable a longer lifetime and more efficient cooling (due to the heat being transferred to water rather than air). For the GHs this was optional as the additional heat may be useful in colder months to reduce heating requirements. To increase this effect and achieve a more consistent light intensity, the LED intensity was adjusted to be highest in the early morning and late evening and progressively dimmed to match the sunlight (SI 1.7). The ratio of photosynthetically active radiation (PAR) received at the canopy compared with the LED output was considered to be slightly higher for plant factories [8].

1.2 Greenhouse cover material selection and orientation

The choice of greenhouse cover material affects both the heat balance and the required supplemental lighting. In colder regions ($T_{average}$ is either < 7.5 C for at least four months or < 0 for at least one month), a high U-value (indicating lower heat transfer to the outside environment) is favourable, and ETFE film (U-value = 2 W/(m²*C), solar transmissitivity 83%) is chosen as a cover. In warmer regions, reduced solar transmissivity is favoured to reduce the mid-day cooling requirements; hence polycarbonate (U-value = 2.27, solar transmissitivity 70%) is chosen as a cover. For arid or desert-like regions with very high average solar radiation and temperatures, a system with aluminium cover panels and refraction lenses (refraction lens cover or RLC) is chosen according to the concept by Pakari and Ghani (2019). The latter is chosen when for more than three months $\frac{DLI_{natural,GH}}{DLI_{required}} > \frac{1}{\frac{\tau_{lens}}{\tau_{cover} * f_{shading}}}$ is given. Both the PC and RLC cover are more resistant to dust and sand particles prevalent in warmer regions. It was assumed that the cover contain an anti-drop layer to stop condensation on the cover material due to temperatures below the dew point of the cover [1]. Besides the cover material, the orientation and geometry play a role in the energy-efficiency of greenhouses, with East-West facing greenhouses showing better utilisation of solar energy [1]. Further, a sturdy wall on the side not facing the sun (North for above the equator and South for below) does not diminish natural light use efficiency while providing heat retention benefits [1]. The HVAC system in this study is considered to be located along the side facing away from the sun.

1.3 Dimensions

The dimensions of the facility and the air conditioning equipment need to be harmonised to ensure adequate performance [9]. The growing area directly determines how much water the plants evaporate and the outside walls determine the heat exchange with the environment. Plant factories have a higher total evaporation per unit floor area due to the stacked growing beds, while GHs have a more pronounced exchange with the environment. The dimensions in this work were thus set to reflect similar duties of the air conditioning units by fixing the volume and having a somewhat larger growing area in the plant factory.

1.4 Seasonal whitewash

Besides the appropriate choice of cover material for given climatic conditions, seasonal whitewash has the potential to reduce energy requirements by reducing the cooling requirements in summer months [10]. It is considered applied in a particular month for ETFE and PC covers if $DLI_{natural} > 1/f_{whitewash,strong}$, if not then $DLI_{natural} > 1/f_{whitewash,light}$.

1.5 Thermal screen

A thermal screen within the greenhouse reduced the heat lost to the environment in colder regions and months. The heuristics are inspired by Vanthoor et al. [5] and assume that at night and very low solar irradiation levels (<15 W m^{-2}), the thermal screens are up as soon as $T_{center} - T_{outside} > 2.5$. During the day, the West (morning until noon) and East (afternoon) facing wall have screens up when $T_{center} - T_{outside} > 10$.

1.6 Natural ventilation

Greenhouse ventilation with outside air is a cost-effective way of climate regulation [5,12–14]. The potential to rely on natural ventilation depends on local wind speeds, buoyancy effects and the design of the vent openings [15,16]. To be able to compare the performance of climate control systems between locations, a uniform wind speed of 2 m/s was assumed which results with typical vent openings in roughly four air exchanges per hour [17]. Further venting flow needs to be supplied with fans. Venting was also possible in the open greenhouse.

1.7 LED lighting schedule, efficiency and direct cooling

Plant growth strongly depends on adequate light supply; increasing the average amount of light received leads to greater photosynthesis (up to a certain point) and thus the synthesis of sugars and other non-structural components which in the end increase the structural biomass generated [18]. In this study, it was considered that greenhouse growers prefer to obtain high yield values per unit area and thus employ artificial lighting. Reference yield values, together with the daily light integral (in mol of photons per day) at which they were obtained, are used to determine the overall lighting requirement (DLI_{plant}). A comparison with the naturally available sunlight on a specific day ($DLI_{natural}$) determines the amount of additional light or moles of light required. It seems that the total amount supplied per day matters more than at which hour they are supplied [2]. At the same time, low solar radiation in the morning and early evening might hamper growth and shorten the effective photoperiod for a specific crop [19]. Thus, the LEDs in greenhouses are considered to supply light in precisely those times at varying intensities to smooth the incoming light profile of the sun, which itself follows a positive sin curve. The following method was devised to obtain the I_{LED} or LED light output in W/m2 from the required DLI_{LED} or daily total light (i.e. photosynthetically active radiation, PAR) output. This will approximate the inverse of the solar radiation, dimming the intensity towards solar noon and increasing it again in the afternoon.

Step 1: From the daily solar radiation curves (see SI in Weidner and Yang (2019) , calculate the total (in Wh/(m^2*day)) and maximum (in Wh/h) solar radiation (only PAR component).

Step 2: Calculate the total Wh to be supplied by the LED (from mol/(m^2*day) to Wh/(m^2*day), Eq.S1).

$$\sum_{0}^{23} I_{LED} = DLI_{LED} * \frac{222000 \frac{J}{mol}}{3600 \frac{s}{h}} \qquad \textit{Eq. S1}$$

Step 3: Add the PAR component of the solar radiation and the total LED output (PAR) and divide it by the photoperiod to obtain an assumed target intensity $I_{target,1st}$ (in W).

Step 4: The resulting target intensity value $I_{target,1st}$ is then used to plot the first approximation of the intensity with equation S2. If the maximum of the solar radiation is lower than this target value, the first approximation will be the actual intensity.

$$I_{LED,1st} = I_{target,1st} - I_{solar,eff} * 0.45 \frac{mol\ PAR}{mol\ solar} \qquad \textit{Eq. S2}$$

Step 5: If this is not the case, then all negative $I_{LED,1st}$ values are added, their hour count defined as N and subtracted from $I_{target,1st}$ as shown in equation S3.

$$I_{target,2nd} = I_{target,1st} - \frac{I_{excess}}{t_{photo} - N} \quad \textit{Eq. S3}$$

Step 6: The second target intensity then determines the LED output by equation S4.

$$I_{LED,2nd} = I_{target,2nd} - I_{solar,eff} * 0.45 \frac{mol\ PAR}{mol\ solar} \quad \textit{Eq. S4}$$

The below figures illustrate this concept for the first and second case (Figure S1 and S2).

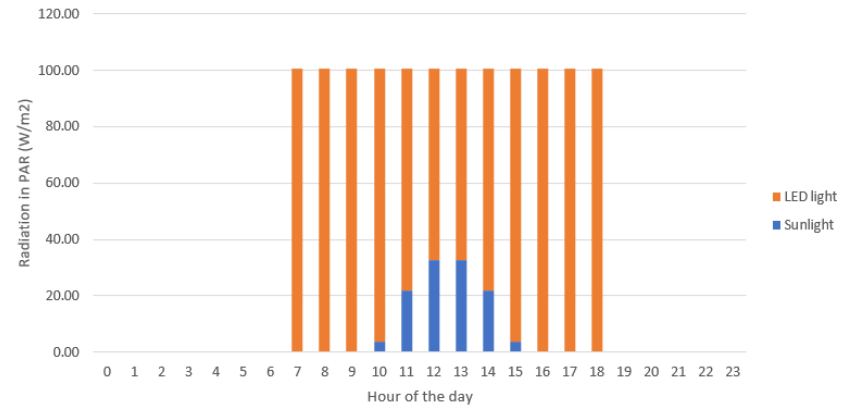

Figure S1: Illustrative hourly radiation composed of LED light and sunlight if the average radiation was above the maximum solar radiation

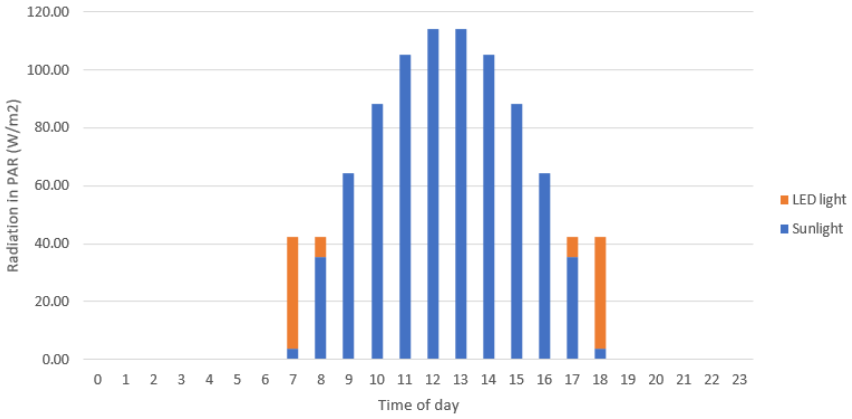

Figure S2: Illustrative hourly radiation composed of LED light and sunlight if the average radiation was below the maximum solar radiation

The standard efficiency, i.e. their ability to convert electrons into photons rather than heat, used in this study is 59% or 2.7 µmol/J which is the average of current models from the largest producers https://www.heliospectra.com/mitra-commercial-led-grow-lights, https://fluence.science/products/spydr-series/ ,

https://www.assets.signify.com/is/content/PhilipsLighting/Assets/philips-lighting/global/20190829-philips-lighting-ps_production_module_3.0_en_final-4.pdf). The efficiency is derived from the conversion factor 4.57 (https://www.controlledenvironments.org/wp-content/uploads/sites/6/2017/06/Ch01.pdf) for light with a wavelength of 400 to 700 nm. LEDs which emit light on a specific wavelength have a different conversion factor, ranging from 3.9 to 5.5 micromol per Joule (https://edepot.wur.nl/156931). In this study it was assumed that plants receive the full spectrum of photosynthetically active radiation.

Beneficial for climate control, this also means the highest amount of waste heat is produced when the greatest (or lowest) requirements for heating (or cooling) occur. In situations where additional waste heat would be an additional burden on the HVAC system (e.g. always in plant factories and in hot months in greenhouses), direct water cooling with an efficiency of up to 85% would be applied and its extent is determined by the optimisation. In plant factories, the DLI was distributed equally between the photoperiod as no synergy with solar energy is required.

2 Mass and energy balances and general equations

2.1 Primary mass and energy balances

The physical behaviour of matter and energy flows in greenhouses and plant factories is not as straightforward as in idealised volumes, such as perfectly mixed spaces or spaces with a uniform gradient along the direction of flow (i.e. plug flow). Many greenhouse climate models assume a perfectly mixed space ([1,21–23] but this is not confirmed by studies applying computational fluid dynamics (CFD) [14,15,24–26] or multi-location measurements [27,28]. We are not aware of studies assuming plug flow reactor (PFR) behaviour for the interior climate, although gradients of temperature and humidity were shown to exist in the previously mentioned CFD studies. The aim of our model is to reflect observed behaviour as closely as possible, while utilising simplifications which enable the optimisation varying internal setpoints and dependent on varying outside climate conditions.

Thus, our methodology approximates the physical behaviour as:

- A well-mixed space (equivalent to a continuously stirred tank reactor or CSTR) at very low venting and AHU flowrates
- A temperature and humidity gradient, i.e. PFR behaviour, for high venting flowrates
- A combination of CSTR and PFR behaviour for medium flowrates, with a more pronounced PFR behaviour for venting (which is typically uni-directional) and a weaker PFR behaviour for the HVAC flow (which is typically introduced at distributed locations within the facility)

This makes it possible to account for different temperature and humiditiy zones within a greenhouse, which have an effect on plant growth and thus need to be kept within a certain range. Thus inlet, centre and outlet conditions are separately evaluated; the inlet zone is representative for growing space close to the fresh (venting) or conditioned (HVAC) air outlet and the outlet zone is representative for growing space close to the vent outlets or the HVAC inlet. Additionally, the conditions at the previous timestep (i.e. thermal and mass inertia) were considered as well and play a more pronounced role for lower venting and HVAC flows, effectively emulating a dynamic system.

The energy balance considers the enthalpy of the CEA facility at the inlet and outlet of the HVAC system and vent openings and can be written as a first order differential equation S5.

$$\frac{dH_{air}}{dt} = F_{vent} * \left(h_{air,outside} - h_{air,out}\right) + F_{hvac} * \left(h_{air,hvac,out} - h_{air,out}\right) + Q_{total} \qquad \textit{Eq. S5}$$

where $\frac{dH_{air}}{dt}$ is the change of enthalpy of the air (including both the dry air and the water vapour) in the space for growing, $h_{air,outside}$ is the outside air enthalpy, $h_{air,hvac,out}$ is the enthalpy of the HVAC outlet air. $h_{air,out}$ is the enthalpy of air at both the inlet of the HVAC system and the outlet of the vents. In practice, those would not necessarily be at exactly the same locations but for simplicity an average outlet condition is adopted for this zone. Q_{total} is the net enthalpy change introduced to the space for growing due to energy or mass flows other than the HVAC and venting air flow. For the PF, CGH and the OGH if venting was off, this would simplify to equation S6.

$$\frac{dH_{air}}{dt} = F_{hvac} * (h_{air,hvac,out} - h_{air,out}) + Q_{total} \quad \text{Eq. S6}$$

In our model implementation, the differential term was approximated by the finite difference method (equation S7)

$$\frac{dH_{air}}{dt} \approx (h_{air,center,t} * Vol * \rho_{dry,center,t} - h_{air,center,t-1} * Vol * \rho_{dry,center,t-1})/\Delta t \quad \text{Eq. S7}$$

where Δt is the interval from time t-1 to time t, which was set to 1 hour or 3600 s. The density used here is the dry air density. The calculation of centre and inlet conditions are based on achieving the above stated aims of the model. The enthalpy at the centre zone of the growing space is defined as shown in equation S8.

$$h_{air,centre} \approx \left(h_{air,outside} * \frac{1}{2} + h_{air,out} * \frac{1}{2}\right) * \frac{F_{vent}}{F_{hvac} + F_{vent} + \frac{Vol * \rho_{dry,centre}}{3600}} + \left(h_{air,hvac,out} * \frac{1}{4} + h_{air,out} * \frac{3}{4}\right) * \frac{F_{hvac}}{F_{hvac} + F_{vent} + \frac{Vol * \rho_{dry,centre}}{3600}} + h_{air,out} * \frac{\frac{Vol * \rho_{dry,centre}}{3600}}{F_{hvac} + F_{vent} + \frac{Vol * \rho}{3600}} \quad \text{Eq. S8}$$

The same relationship is used for the other air properties (density, specific humidity and temperature) by replacing the enthalpy term with the respective property. Akin to the centre zone, the inlet zone is defined as shown in equation S9.

$$h_{air,inlet} \approx h_{air,outside} * \frac{F_{vent}}{F_{hvac} + F_{vent} + \frac{Vol * \rho_{dry,centre}}{3600}} + \left(h_{air,hvac,out} * \frac{1}{2} + h_{air,out} * \frac{1}{2}\right) * \frac{F_{hvac}}{F_{hvac} + F_{vent} + \frac{Vol * \rho_{dry,centre}}{3600}} + h_{air,out} * \frac{\frac{Vol * \rho_{dry,centre}}{3600}}{F_{hvac} + F_{vent} + \frac{Vol * \rho_{dry,centre}}{3600}} \quad \text{Eq. S9}$$

The first terms in equation S8 and S9 describe the influence of venting on the zone (with a more pronounced PFR behaviour), the second term describe the influence of the HVAC outlet into the growing space (with a combined PFR and well-mixed space behaviour) and the third term accounts for the well-mixed space behaviour at low venting and HVAC flowrates. The inlet zone relation was used in the optimisation to derive the temperature dependent yield factor (see SI 4.2) and the adherence to climate setpoints (e.g. keeping the vapour pressure deficit between 0.4 and 1.2 kPa) in this zone.

Equation S8 was then combined with equation S6 and equation S7 to derive the energy balance valid for all systems, equation S10 (ρ was used here to describe $\rho_{dry,centre}$):

$$F_{vent} * \left(h_{air,outside} - h_{air,out}\right) + F_{hvac} * (h_{air,hvac,out} - h_{air,out}) + Q_{total} = \quad \text{Eq. S10}$$

$$\left(\left(h_{air,outside} * \frac{1}{2} + h_{air,out} * \frac{1}{2}\right) * \frac{F_{vent}}{F_{hvac} + F_{vent} + \frac{Vol * \rho}{3600}} + \left(h_{air,hvac,out} * \frac{1}{4} + h_{air,out} * \frac{3}{4}\right) * \frac{F_{hvac}}{F_{hvac} + F_{vent} + \frac{Vol * \rho}{3600}} + h_{air,out} * \frac{\frac{Vol * \rho}{3600}}{F_{hvac} + F_{vent} + \frac{Vol * \rho}{3600}}\right) * \frac{Vol * \rho}{3600} - \frac{h_{air,center,t-1} * Vol * \rho_{t-1}}{3600}$$

Which can be simplified to Eq S11 if there is no venting.

$$F_{hvac} * (h_{air,hvac,out} - h_{air,out}) + Q_{total} = \quad \text{Eq. S11}$$

$$\left(\left(h_{air,hvac,out}*\frac{1}{4}+h_{air,out}*\frac{3}{4}\right)*\frac{F_{hvac}}{F_{hvac}+\frac{Vol*\rho}{3600}}+h_{air,out}*\frac{\frac{Vol*\rho}{3600}}{F_{hvac}+\frac{Vol*\rho}{3600}}\right)*\frac{Vol*\rho}{\Delta t}$$
$$-\frac{h_{air,center,t-1}*Vol*\rho_{t-1}}{\Delta t}$$

Rearranging for $h_{air,out}$

$$h_{air,out}=\frac{h_{air,center,t-1}*Vol*\rho_{t-1}-Vol*\rho\left(\frac{0.5*h_{air,outside}*F_{vent}*+0.25*h_{air,hvac,out}*F_{hvac}}{F_{hvac}+F_{vent}+\frac{Vol*\rho}{3600}}\right)}{3600*\left(F_{vent}+F_{hvac}+\left(\frac{0.5*F_{vent}+0.75*F_{hvac}+\frac{Vol*\rho}{3600}}{F_{hvac}+F_{vent}+\frac{Vol*\rho}{3600}}\right)*\frac{Vol*\rho}{3600}\right)}$$
$$+\frac{F_{vent}*h_{air,outside}+F_{hvac}*h_{air,hvac,out}+Q_{total}}{\left(F_{vent}+F_{hvac}+\left(\frac{0.5*F_{vent}+0.75*F_{hvac}+\frac{Vol*\rho}{3600}}{F_{hvac}+F_{vent}+\frac{Vol*\rho}{3600}}\right)*\frac{Vol*\rho}{3600}\right)} \quad \textit{Eq. S12}$$

Equation S12 can be simplified for the case of F_{vent} = 0 (equation S13).

$$h_{air,out}=\frac{h_{air,center,t-1}*\frac{Vol*\rho_{t-1}}{3600}-\left(\frac{0.25*h_{air,hvac,out}*F_{hvac}}{F_{hvac}+\frac{Vol*\rho}{3600}}\right)\frac{Vol*\rho}{3600}+F_{hvac}*h_{air,hvac,out}+Q_{total}}{\left(F_{hvac}+\left(\frac{0.75*F_{hvac}+\frac{Vol*\rho}{3600}}{F_{hvac}+\frac{Vol*\rho}{3600}}\right)*\frac{Vol*\rho}{3600}\right)} \quad \textit{Eq. S13}$$

Similar to the energy balance, the mass balance for water incorporates the specific humidity ω in g water vapour per kg air at the centre zone, as well as the infiltration balance and the added water vapour from evapotranspiration and fogging (equations S14 and S15).

$$\frac{dm_w}{dt}=(\omega_{outside}-\omega_{out})*F_{vent}+(\omega_{hvac,out}-\omega_{out})*F_{hvac}+m_{w,evap}+\left[m_{w,fog}+m_{w,infiltration}\right] \quad \textit{Eq. S14}$$

$$\frac{dm_w}{dt}\approx(\omega_{center,t}*Vol*\rho_{center,t}-\omega_{center,t-1}*Vol*\rho_{center,t-1})/\Delta t \quad \textit{Eq. S15}$$

The specific humidity in the centre zone is defined analogous to the enthalpy (equation S16).

$$\omega_{centre}\approx\left(\omega_{outside}*\frac{1}{2}+\omega_{out}*\frac{1}{2}\right)*\frac{F_{vent}}{F_{hvac}+F_{vent}+\frac{Vol*\rho_{dry,centre}}{3600}}+\left(\omega_{hvac,out}*\frac{1}{4}+\omega_{out}*\frac{3}{4}\right)$$
$$*\frac{F_{hvac}}{F_{hvac}+F_{vent}+\frac{Vol*\rho_{dry,centre}}{3600}}+\omega_{air,out}*\frac{\frac{Vol*\rho}{3600}}{F_{hvac}+F_{vent}+\frac{Vol*\rho_{dry,centre}}{3600}} \quad \textit{Eq. S16}$$

The specific humidity at the inlet is consequently defined as shown in equation S17.

$$\omega_{inlet}\approx\omega_{outside}*\frac{F_{vent}}{F_{hvac}+F_{vent}+\frac{Vol*\rho_{dry,centre}}{3600}}+\left(\omega_{hvac,out}*\frac{1}{2}+\omega_{out}*\frac{1}{2}\right)*\frac{F_{hvac}}{F_{hvac}+F_{vent}+\frac{Vol*\rho_{dry,centre}}{3600}}$$
$$+\omega_{out}*\frac{\frac{Vol*\rho}{3600}}{F_{hvac}+F_{vent}+\frac{Vol*\rho_{dry,centre}}{3600}} \quad \textit{Eq. S17}$$

Which means that Equations S14 to S16 combine to Equation S18 below, similarly to the enthalpy (again ρ was used here to describe $\rho_{dry,centre}$).

$$\omega_{out} = \frac{\omega_{center,t-1} * Vol * \rho_{t-1} - Vol * \rho \left(\frac{0.5 * \omega_{outside} * F_{vent} * +0.25 * \omega_{hvac,out} * F_{hvac}}{F_{hvac} + F_{vent} + \frac{Vol * \rho}{3600}} \right)}{3600 * \left(F_{vent} + F_{hvac} + \left(\frac{0.5 * F_{vent} + 0.75 * F_{hvac} + \frac{Vol * \rho}{3600}}{F_{hvac} + F_{vent} + \frac{Vol * \rho}{3600}} \right) * \frac{Vol * \rho}{3600} \right)} + \frac{F_{vent} * \omega_{outside} + F_{hvac} * \omega_{hvac,out} + m_{w,evap} + [m_{w,fog} + m_{w,infiltration}]}{\left(F_{vent} + F_{hvac} + \left(\frac{0.5 * F_{vent} + 0.75 * F_{hvac} + \frac{Vol * \rho}{3600}}{F_{hvac} + F_{vent} + \frac{Vol * \rho}{3600}} \right) * \frac{Vol * \rho}{3600} \right)} \quad \text{Eq. S18}$$

The temperature at the HVAC inlet can now be calculated with equation S19 derived from equation S20 (accurate in the temperature region of interest).

$$T_{air,out} = \frac{h_{air,out} - 2.5 * \omega_{out}}{1.01 + 0.00189 * \omega_{out}} \quad \text{Eq. S19}$$

$$h_{air} = T_{air} * (1.01 * 0.00189 * \omega) + 2.5 * \omega \quad \text{Eq. S20}$$

The total amount of energy into the room is described by equation S21, Q_{solar} and $Q_{inflitration}$ are specific to GHs.

$$Q_{total} = \left(Q_{structure} + Q_{LED,PAR} + Q_{LED,heat} + Q_{SH} + Q_{fans,hvac} + [Q_{solar} + Q_{inflitration}]\right) + h_{w,T_{center}} * m_{w,fog} + h_{sat,T_{leaf}} * m_{w,evap} \quad \text{Eq. S21}$$

The total energy to be added or removed in the HVAC is calculated by equations S22 and S23.

$$Q_{cool,req} = \begin{cases} F_{hvac} * \left(h_{air,GH,out} - h_{air,equiv}\right) - m_{w,out} * h_{w,T_{equiv}} & if\ m_{w,out} > 0\ and\ h_{air.GH,out} > h_{air,hvac,out} \\ F_{hvac} * \left(h_{air,GH,out} - h_{air,hvac,out}\right) & if\ m_{w,out} = 0\ and\ h_{air.GH,out} > h_{air,hvac,out} \\ 0 & else \end{cases} \quad \text{Eq. S22}$$

$$Q_{heat,req} = \begin{cases} F_{hvac} * \left(h_{air,hvac,out} - h_{air,equiv}\right) & if\ m_{w,out} > 0 \\ F_{hvac} * \left(h_{air,hvac,out} - h_{air,GH,out}\right) & if\ m_{w,out} = 0\ and\ \ h_{air,hvac,out} > h_{air,GH,out} \\ 0 & else \end{cases} \quad \text{Eq. S23}$$

In the PF with continuous dehumidification, these simplify to equations S24 and S25.

$$Q_{cool,req} = F_{hvac} * \left(h_{air,hvac,in} - h_{air,equiv}\right) - m_{w,out} * h_{w,T_{equiv}} \quad \text{Eq. S24}$$

$$Q_{heat,req} = F_{hvac} * \left(h_{air,hvac,out} - h_{air,equiv}\right) \quad \text{Eq. S25}$$

2.2 Exchanges with the environment

To calculate Q_{total}, the following equations are employed (Eq. S26 to S33).

$$U_{GH} = \frac{U_{cover} * \left(A_{Roof} * f_{screen} + A_{wall,S} * f_{screen} + A_{walls,E,W} * \left(1 + f_{screen,EW}\right) * 0.5\right) + U_{wall} * A_{wall,N}}{A_{Roof} + A_{facade}} \quad \text{Eq. S26}$$

$$Q_{GH} = Q_{structure} = U_{GH} * (T_{outside} - T_{center}) * (A_{roof} + A_{facade}) * (1 + f_{radiation}) \quad \text{Eq. S27}$$

$$Q_{PF} = Q_{structure} = U_{wall} * \left(T_{air,outside} - T_{air,center}\right) * \left(A_{roof} + A_{facade}\right) \quad \text{Eq. S28}$$

$$Q_{solar} = I_{solar,eff} * \left(1 - f_{production}\right) * A_{roof} + \left(I_{solar,eff} + I_{LED} - I_{net}\right) * A_{growing} \quad \text{Eq. S29}$$

Source: [7,17]

$$A_{growing} = A_{roof} * f_{production} * N_{racks} \quad \text{Eq. S30}$$

$$Q_{LED,PAR} = I_{LED} * \left(\left(1 - CAC\right) + e^{-k_s * LAI} + \left(1 - \frac{PAR_{Plant}}{PAR_{LED}}\right)\right) * A_{growing} \quad \text{Eq. S31}$$

Source: [29–31]

Note: The above equations ensure that solar radiation and PAR not absorbed by plants are not double-counted in the energy balance.

$$Q_{LED,heat} = \left(Power_{LED} - I_{LED}\right) * A_{growing} * \left(1 - f_{LED\ cooling}\right) \quad \text{Eq. S32}$$

$$Q_{cool,LED} = \left(Power_{LED} - I_{LED}\right) * A_{growing} * \left(f_{LED\ cooling}\right) \quad \text{Eq. S33}$$

The energy and mass balance of infiltration and fogging are shown in equation S34 to S36.

$$Q_{infiltration} = AER_{infiltration} * Vol * \rho_{outside} * \left(1 - \frac{\omega_{outside}}{1000 + \omega_{outside}}\right) * \frac{h_{air,outside} - h_{air,center}}{3600} \quad \text{Eq. S34}$$

Note: Q_infiltration already includes the balance enthalpy of in- and outgoing water vapour, hence it is excluded in Q_total. The specific enthalpy of air adopted here is per unit mass of dry air, hence $\rho_{outside}$ of wet air needs to be converted to the density of dry air (kg dry air per unit volume of air flow) using the specific humidity.

$$m_{w,balance,infiltration} = AER_{infiltration} * Volume * \rho_{centre} * \left(\omega_{centre} - \omega_{outside}\right) \quad \text{Eq. S35}$$

$$E_{fog} = m_{w,fog} * 3600 * \frac{E_{fog,ref}}{\eta_{fog}} \quad \text{Eq. S36}$$

The resource loss is shown by equations S37 to S39.

$$m_{CO2,loss,infiltration} = \frac{P_{atm} * Vol * AER_{infiltration}}{R * \left(T_{centre} + 273\right)} * \frac{C_{CO2,centre} - C_{CO2,ambient}}{1000000 \frac{1}{mol}} * \frac{MW_{CO2}}{1000 \frac{g}{kg}} \quad \text{Eq. S37}$$

Note: There is no CO_2 loss at night as the interior air is only conditioned during the photo period. In the OGH, $CO_{2,centre}$ becomes $CO_{2,centre-1}$ to avoid a circular reference without significant impact on the results.

$$m_{w,balance,OGH} = m_{w,balance,infiltration} + F_{vent,dry} * \left(\omega_{GH,out} - \omega_{outside}\right) \quad \text{Eq. S38}$$

Due to the dehumidification device, more water vapour from the outside might be condensed than what is being lost (e.g. if the outside air is very humid). To account for potentially negative and positive $m_{w,balance,infiltration}$ values, the balance values over the 24 hours are added up to obtain the loss.

$$m_{w,loss} = \sum_{1}^{24} m_{w,balance} * 3600 \frac{s}{h} \quad \text{Eq. S39}$$

The irrigation water that is used by the plant for biomass growth is not considered in this study as it will be the same for the three systems. For the CGH, the ventilation represents additional exchange with the environment; the air velocity was calculated by equation S40 [9] and pressure drop and fan electricity by equations S41 and S42.

$$u_{vent,out} = \frac{F_{vent} * \left(1 + \frac{\omega_{GH,out}}{1000\frac{g}{kg}}\right)}{\rho_{GH,out} * A_{sect} * f_{vent\ size}} \quad \text{Eq. S40}$$

$$\Delta P_{vent} = u_{vent,out}^2 * \frac{\rho_{GH,out}}{2} + 3.4 * u_{vent,out}^2 + 4.9 * u_{vent,out} \quad \text{Eq. S41}$$

$$E_{fans,vent} = \begin{cases} \frac{F_{vent}}{\rho_{outside}} * \frac{AER_{vent} - 4}{AER_{vent}} * \frac{\Delta P_{vent}}{\eta_{fans}} & if\ AER_{vent} > 4 \\ 0 & else \end{cases} \quad \text{Eq. S42}$$

Note: For AER_vent <= 4/h natural ventilation was assumed (according to calculations with wind speeds of 2 m/s.

2.3 Carbon dioxide level in the open greenhouse

The CO_2 level at the centre was calculated using equations S43 to S46 for the OGH.

$$\frac{dn_{CO2}}{dt} = C_{CO2,outside} * n_{air,vent} + \frac{\left(m_{CO2,supply} - m_{CO2,loss,infiltration}\right) * \frac{1000g}{kg}}{MW_{CO2}} - C_{CO2,centre} * n_{air,vent} \quad \text{Eq. S43}$$

$$n_{air,vent} = \frac{F_{vent} * 1000\frac{g}{kg}}{MW_{air}} \quad \text{Eq. S44}$$

$$\frac{dn_{CO2}}{dt} \approx \frac{\left(C_{CO2,centre} - C_{CO2,centre-1}\right) * \frac{Vol * P_{atm}}{R * (T_{centre} + 273)}}{\Delta t} \quad \text{Eq. S45}$$

$$C_{CO2,centre} = \frac{C_{CO2,outside} * n_{air,vent} + \frac{\left(m_{CO2,supply} - m_{CO2,loss,infiltration}\right) * \frac{1000g}{kg}}{MW_{CO2}} + C_{CO2,centre-1} * \frac{Vol * P_{atm}}{R * (T_{centre} + 273)} * 3}{\frac{Vol * P_{atm}}{R * (T_{centre} + 273)} * \frac{1}{3600} + n_{air,vent}} \quad \text{Eq. S46}$$

The CO_2 supply during the photoperiod with venting in the OGH was regulated in order to balance CO_2 purchase cost and environmental impact with the increase in yield, while ensuring that it would not be lower than in the closed greenhouse if there was no venting (equation S47).

$$m_{CO2,supply} = Y_{hourly}@1600ppm@T_{opt} * 0.3 + m_{CO2,loss,infiltration} \quad \text{Eq. S47}$$

$$m_{CO2,supply} \leq \left(C_{CO2,target} - C_{CO2,outside}\right) * n_{air,vent} * MW_{CO2} * \frac{3600\frac{s}{h}}{1000\frac{g}{kg}} + \left(C_{CO2,target} - C_{CO2,center-1}\right) * \frac{Vol * P_{atm}}{R * (T_{centre} + 273)} * \frac{MW_{CO2}}{1000\frac{g}{kg}} * + m_{CO2,loss,infiltration} \quad \text{Eq. S48}$$

Equation S48 ensures that at no time more CO_2 is supplied than needed to maintain the target CO_2 concentration. The 0.3 kg CO_2/kg edible crop produced is derived from Hemming et al. [32] to reflect current best practice.

For the CGH, we found that the loss of CO_2 through the low infiltration rate could be compensated by typical CO_2 dosing rates even at 1600 ppm while staying in the range of kg CO_2/kg crop values reported by Hemming et al. [32]. The CO_2

level during the photo period was thus fixed in the CGH and supply would cease in the dark period to prevent wasting CO_2 when it does not increase plant growth. Equation S49 thus simplifies in the dark period to

$$C_{CO2,centre} = \frac{\left(m_{CO2,loss,infiltration}\right) * \frac{1000g}{kg}}{\frac{MW_{CO2}}{\frac{Vol * P_{atm}}{R * (T_{centre} + 273)} * \frac{1}{3600} +}} + C_{CO2,centre-1} * \frac{Vol * P_{atm}}{R * (T_{centre} + 273)} * \frac{1}{3600} \quad \text{Eq. S49}$$

The required supply to boost the CO_2 concentration at the beginning of the photoperiod is described by equation S50 for both GHs.

$$m_{CO2,supply}@t(photo) = \frac{C_{CO2,target} - C_{CO2,centre-1}@t(photo) - 1}{1000000 \frac{ppm}{mol}} * \frac{Vol * P_{atm}}{R * (T_{centre} + 273)} * \frac{MW_{CO2}}{1000 \frac{g}{kg}} \quad \text{Eq. S50}$$

In the case of the OGH, any ventilation flowrate determined by the optimisation higher than zero at 7 AM will lead to an initial CO_2 level below the target CO_2 level.

For the CGH, the total CO_2 supplied (and lost to the air) can be calculated for the day (except the first hour) with equation S51:

$$m_{CO2,supply} = m_{CO2,loss,infiltration} \quad \text{Eq. S51}$$

The mass of CO2 that needs to be supplied for plant growth was not considered in this study as it will be the same for all three systems (in terms of kg CO_2/kg produce) and typically discounted as biogenic in life cycle assessments of food system impacts.

2.4 Thermodynamic relations

Equations S52 to S66 describe the behaviour of water vapour in air

$$\omega = 622 * \frac{P_w}{P_{atm} - P_w} \quad \text{Eq. S52}$$

$$P_{sat} = 6.116 * 10^{7.591 * \frac{T}{T+240.73}} \quad \text{Eq. S53}$$

$$X = 216.68 * \frac{P_w}{T + 273} \quad \text{Eq. S54}$$

$$RH = \frac{P_w}{P_{sat}} \quad \text{Eq. S55}$$

Source: https://www.hatchability.com/Vaisala.pdf

$$\rho = \frac{P * 100}{R_a * (T + 273)} * \frac{1 + \omega * 1000}{1 + \omega * 1000 * \frac{R_w}{Ra}} \quad \text{Eq. S56}$$

Source: https://www.engineeringtoolbox.com/density-air-d_680.html

$$h_{sat} = (2676 - (100 - T) * 1.7266) \quad \text{Eq. S57}$$

$$\lambda = 2501 - 2.361 * T \quad \text{Eq. S58}$$

$$X_{air} = \omega_{air} * \rho_{air} \quad \text{Eq. S59}$$

$$h_w = C_w * T_{air} \quad \text{Eq. S60}$$

$$X_{leaf} = P_{sat,T_{leaf}} * 100 * \frac{18\ \frac{g\ H_2O}{mol}}{R * (T_{leaf} + 273)} \quad \text{Eq. S61}$$

$$VPD_{leaf} = P_{sat,T_{leaf}} - P_{w,center} \quad \text{Eq. S62}$$

$$VPD_{air} = P_{sat} - P_w \quad \text{Eq. S63}$$

$$VCD = X_{leaf} - X_{center} \quad \text{Eq. S64}$$

$$T_{air,equiv} = \frac{\log\frac{P_{w,hvac,out}}{6.116}}{7.591} * 240.7 \quad \text{Eq. S65}$$
$$1 - \frac{\log\frac{P_{w,hvac,out}}{6.116}}{7.591}$$

Note: Rearranged saturated vapour pressure equation

$$P_{w,hvac,in} = \frac{X_{hvac,in}}{216.68} * (273 + T_{air,hvac,in}) \quad \text{Eq. S66}$$

Additionally, equation S67 to S72 describe the remaining mass and energy balances, equation S73 the pressure drop in the duct and equation S74 the electricity consumption of the fans.

$$u_{air,center} = (F_{hvac} + F_{vent}) * \frac{1 + \frac{\omega_{center}}{1000}}{\rho_{center} * A_{sect}} \quad \text{Eq. S67}$$

$$V_{hvac} = \frac{F_{hvac} * \left(1 + \omega_{hvac,out}\right)}{\rho_{hvac,out}} \quad \text{Eq. S68}$$

$$AER_{hvac} = \frac{V_{hvac} * 3600}{Vol} \quad \text{Eq. S69}$$

$$m_{w,evap} = ET * \frac{A_{growing}}{3600} \quad \text{Eq. S70}$$

$$m_{w,out} = F_{hvac} * \left(\omega_{hvac,in} - \omega_{hvac,out}\right) * \frac{1\ kg}{1000\ g} \quad \text{Eq. S71}$$

$$u_{air,hvac} = \frac{V_{hvac}}{A_{duct}} \quad \text{Eq. S72}$$

$$\Delta P_{hvac} = \frac{(V_{hvac} * 2118.9)^{1.9} * 0.109136}{(D_{duct} * 39.37)^{5.02}} * 8.162 * L_{duct} + \xi * \rho_{hvac,out} * \frac{u_{air,hvac}^2}{2} \quad \text{Eq. S73}$$

Note: Equation from https://www.engineeringtoolbox.com/sizing-ducts-d_207.html, ducts sized for air flows of AER = 10 and 10,000 m3 volume, with a maximum air speed of 12 m/s.

$$E_{fans,hvac} = Q_{fans.hvac} = V_{hvac} * \Delta P_{hvac} * \frac{1}{\eta_{fans}} \quad \text{Eq. S74}$$

Source: [9]

2.5 Physical relations

Equations S75 to S83 describe the variables related to solar radiation and LEDs.

$$I_{solar,eff} = I_{solar,sky} * \tau_{cover} * f_{shading} * f_{whitewash} \quad \text{Eq. S75}$$

Source: [10]

$$DLI_{natural,GH} = \frac{0.45 \frac{mol\ PAR}{mol\ solar}}{222000 \frac{J}{mol\ PAR}} \int_{0\ h}^{24\ h} I_{solar,eff} \quad \text{Eq. S76}$$

$$DLI_{LED,canopy} = DLI_{plant} - DLI_{natural} \quad \text{Eq. S77}$$

$$DLI_{LED} = \frac{DLI_{LED,canopy}}{\frac{PAR_{canopy}}{PAR_{LED}}} \quad \text{Eq. S78}$$

$$I_{LED,canopy} = I_{LED} * \frac{PAR_{canopy}}{PAR_{LED}} \quad \text{Eq. S79}$$

Note: The PAR from the LED is not the same as the PAR reaching the plants. Some of the radiation does not reach the canopy (represented by the ratio in this equation), which can be reduced by reflective surfaces within the facility. Further, radiation is lost when the plant cover of the canopy is below 100%, represented by the CAC value in equation S80.

The calculation steps to get from DLI_{LED} to I_{LED} are described in SI 1.6.

Equations S80 and S81 are then used for the evapotranspiration balance and the calculation of the canopy resistance, respectively.

$$I_{net} = \left(I_{LED,canopy} + I_{solar,eff}\right) * CAC * \left(1 - e^{-k_s * LAI}\right) \quad \text{Eq. S80}$$

Source: [7]

$$I_{net,PAR} = \left(I_{LED,canopy} + I_{solar,eff} * 0.45\right) * CAC * \left(1 - e^{-k_s * LAI}\right) \quad \text{Eq. S81}$$

Source: [31]

$$Power_{LED} = \frac{I_{LED}}{\eta_{LED}} \quad \text{Eq. S82}$$

For the case of constant LED output, equations S83 determined the required photoperiod within one day, split between the morning and late afternoon hours in the greenhouses. The determination of the LED efficiency is explained in section S1.7.

$$t_{photo} = \frac{DLI_{LED,canopy} * 1000000 \frac{\mu mol}{mol}}{PPFD_{LED} * 3600 \frac{s}{h} * \frac{PAR_{canopy}}{PAR_{LED}}} \quad \text{Eq. S83}$$

Finally, the dimensions of the facilities were calculated using equations S84 to S88.

$$Vol = W * L * H \quad \text{Eq. S84}$$

$$A_{roof} = L * W \quad \text{Eq. S85}$$

$$A_{wall,S} = A_{wall,N} = L * H \quad \text{Eq. S86}$$

$$A_{wall,E,W} = A_{sect} = W * H \quad \text{Eq. S87}$$

$$A_{facade} = 2 * H * (W + L) \quad \text{Eq. S88}$$

3 Space conditioning

3.1 Design and concepts of the air handling unit

Ventilation is sometimes either not an option (PF and CGH) or has limited potential to keep climate parameters such as humidity in check, e.g. when the outside air is hotter or more humid than the inside air [7]. This study, therefore, considers a comprehensive air handling unit (AHU) to condition the circulating GH or PF air (see figure S3). It is equipped with an air-to-air heat exchanger ("free" cooling), a refrigeration cycle (RC) for condensing (dehumidification) and cooling of the internal air and an air-source heat pump (ASHP) to either increase air temperature after the condensation step or to simply heat the circulating air. Although ground-source heat pumps can be more efficient, ASHPs were chosen due to their lower upfront investment costs and their global applicability since they are not dependent on shallow, accessible and abundant groundwater. Such integrated AHUs are readily available on the market and can be customised for specific purposes (https://www.aaon.com/Documents/Sales/M2_ONLINE_160419.pdf).

In the PF, the sealed building combined with the evapotranspiration from plants results in permanent dehumidification requirements. Hence, the air in the AHU is cooled below the dew point and subsequently heated up again to the target temperature. In the CGH, the infiltrating air causes the AHU to vary in its operation depending on the circulating flowrate; the air is either dehumidified and heated up again, is simply cooled or heated without any change in the absolute humidity of the air stream (if the moisture removal through infiltration is equal or greater than the evapotranspiration). In the OGH, the AHU works together with the ventilation and fogging system to control the climate. The operation is similar to the CGH, but the AHU is combined with venting operations to reduce the overall energy consumption. Thus, the AHU either dehumidifies (cooling below the dew point with subsequent heating) or simply cools or heats the air, depending on the desired inlet zone conditions.

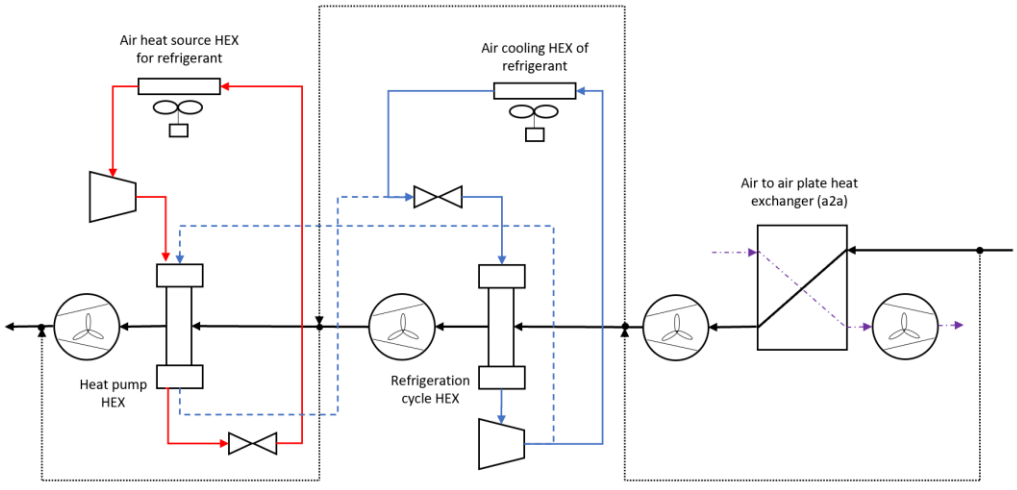

Figure S3: Schematic of the air handlung unit (AHU), including the air-to-air heat exchanger. Blue arrows describe the refrigeration cycle, red arrow the heating circuit. Dotted arrows are the bypass lines.

The electricity consumers of the AHU consist of two compressors (in the RC and ASHP) and several fans to overcome the pressure drop created by the smaller channels in the heat exchangers (see image on the left). There are in total 5 HEXs, i.e. air-to-air, refrigerant evaporator (between internal air and refrigerant) and condenser (between the refrigerant and outside air), ASHP evaporator (between the refrigerant and outside air) and condenser (between internal air and refrigerant). The air-to-air HEX requires two fans (outside and internal air), all other HEXs one internal air and one external air fan (the liquid within the tubes is propelled through the pressure difference created by the compressor). The air-to-air HEX is considered to be a counter-flow plate HEX while all other HEXs are cross-flow finned tube HEX in which the refrigerant circulates within the tubes.

To fully capture the influence of the outside climate and the requirements on the internal air conditioning in the optimisation, the electricity consumption of the six fans and two compressors were made wholly dependent on the cooling and heating load as well as the temperatures and absolute humidity of the AHU inlet, outlet and outside air. Previous studies either optimised the cooling and heating duty without further investigation how this would be realised in an HVAC system [33,34] or indicated the electricity consumption through constant heating and cooling COPs for a specific location [7]. To satisfy the requirements for detail and flexibility, this work builds on the methodology developed by Graamans et al. [9] and incorporates concepts such as a) the NTU method [35] combined with b) a distinction between cooling and cooling with condensation of the internal air in the air-to-air HEX, c) state variable plotting to obtain empirical polynomial equations (e.g. temperature, enthalpy and entropy of the refrigerant in the RC) and d) heat integration between the ASHP and RC condensers.

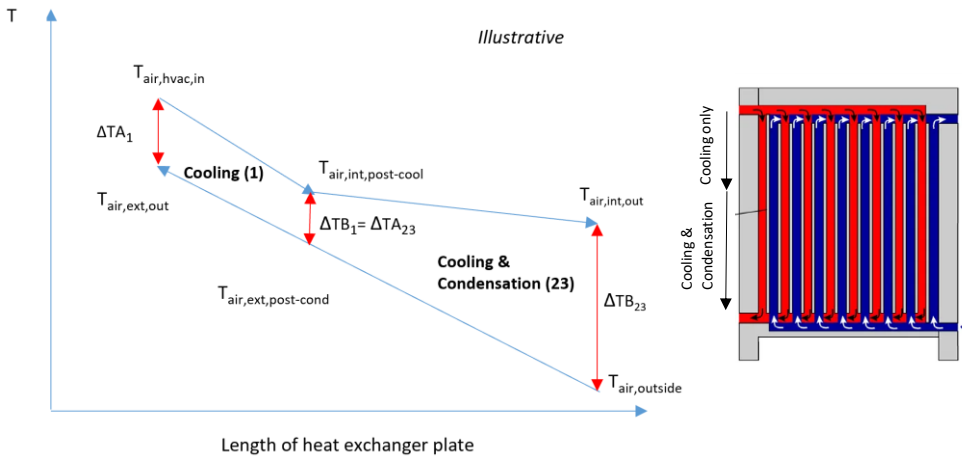

Figure S4: Illustrative T-L diagram of the air-to-air heat exchanger, containing a cooling only zone and a zone in which water vapour is continuously condensed as air is fully saturated. The image on the right illustrates how this would look like in a schematic of a plate heat exchanger (from https://whatispiping.com/plate-heat-exchanger-with-steam-1/)

The air-to-air HEX is added to the system to make use of cold outside air in winter or cold regions. The HEX will need to be able to both cool the internal air to the target temperature and dehumidify it (see figure S4). The latter occurs when the temperature reaches its saturation point for a given absolute humidity and continues until the target absolute humidity is reached (defined as step 23). This process is different from a cooling-only process (defined as step 1) since the heat capacity ratio between the streams differs for the two steps (see figure on the left). An iterative process using the NTU-method was developed to account for this.

1. Based on the value of the decision variables $u_{air,ext}$ (external air velocity) and $f_{a2a,share}$(amount of internal air sent through air-to-air HEX), the model assessed whether the potential duty is higher than the duty required

for step 1 (equations S104 to S114). If so, the area of the HEX was divided by the share of step 1 duty to the potential duty to obtain a cooling ratio splitting the available HEX area (equation S115).

2. The remaining area was used to determine the potential duty for step 23 and the resulting external air temperature after the condensation step (equations S116 to S124).
3. The external air temperature and available HEX area for step 1 were then used to recalculate the step 1 duty (equations S125 and S126).
4. The error between the required duty and the recalculated duty (equation S127) was used to refine the cooling ratio (equation S128).
5. Steps 2 to 4 were repeated 4 times which appeared sufficient to reach a convergence
6. The final cooling ratio was used to determine the actual step 23 duty and thus the remaining cooling duty to be realised by the RC (equations S129 to S134)
7. The value of the decision variables determined the fan power consumption requirements (equations S135 to S138) and the optimisation routine compared those with the energy savings in the RC achieved by the air-to-air HEX, finding the optimum balance between the two options.

The RC was modelled in three steps. First, the outside air and target temperature after the RC, either T_{equiv} (if condensation is required) or $T_{hvac,out}$, were used to determine the operating conditions of the refrigeration cycle, i.e. the evaporator and condenser temperature (equations S139 to S143). Saturated refrigerant properties and a P-t diagram (see below) were used to derive polynomial equations for enthalpy and entropy (depending on temperature values, equations S144 to S151).

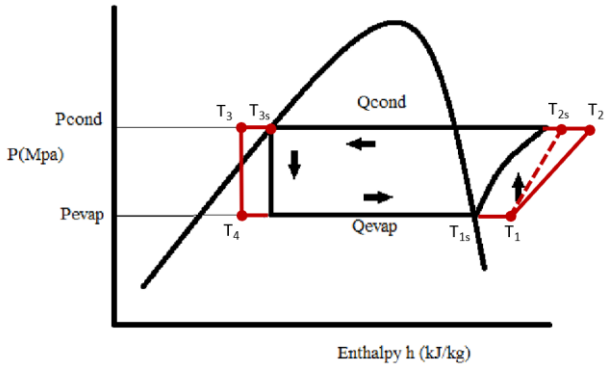

Figure S5: Illustrative P-h diagram of the refrigeration cycle. The red lines describe the subcooling and superheating.

These would then indicate the refrigerant enthalpy at the relevant locations within the RC, allowing to calculate the COP and electricity consumption of the compressor (equations S152 to S155).

Second, the required refrigerant flow (equation S156) determines the cooling requirements in the condenser section (equation S160), which was realised by a) reheating the internal air stream if it was required and desired (equations S161 to 165) and b) by an air-cooled HEX for the remaining part (equations S166 to 168). Reheating the internal stream means a reduced or nullified requirement for the ASHP to reheat the internal air stream (see Figure S3). The optimisation ensured that the most energy-efficient pathway is chosen, balancing "free" air2air cooling (which, if used for the complete cooling requirements, would necessitate the ASHP to deliver all reheating requirements) with refrigerant cycle cooling.

Third, the required outside air flows and thus fan power consumptions were assessed and combined with the power consumption of the internal air fans and the compressor (equations S169 and S170).

The remaining heating duty was to be covered by the ASHP, for which an empirical relation related outside air temperature to the power consumption (equations S171 and S172). This relation was also used when the HVAC was only used for heating. The COP for LED cooling was assessed with fixed inlet and outlet water temperatures as shown in

equation S173. The developed methodology results in similar COP values as indicated by other studies for cooling [8,36] and heating [37,38]. An illustration of the COP of the whole system for a given space conditioning duty for a PF is shown in the figure below.

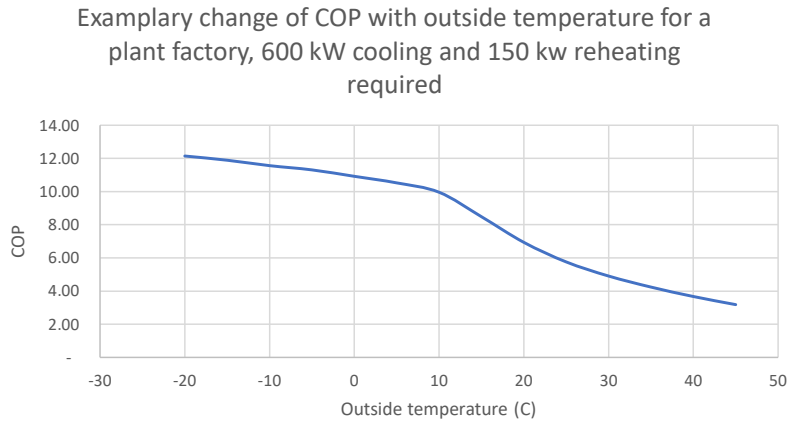

Figure S6: Exemplary coefficient of performance vs. temperature diagram of the refrigeration cycle at full load

All HEXs were designed to cope with the maximum expected heating and cooling duties (around 750 kW) while occupying only a stretch of 2 m along the North wall. This led to relatively large HEX areas which might result in high investment costs. A full economic analysis would be needed to strike a balance between capital investment and energy savings, which is out of the scope of this work. The dimensions of the three types of HEX (counter-flow plate, air to air; cross-flow finned tube, internal air to refrigerant; cross-flow finned tube, refrigerant to external air) are listed below in Table S1.

Table S1: Dimension of the heat exchangers in the air conditioning system

Design air-to-air HEX	**Dimen-sions**	**Design finned tubes of air-to-refrigerant HEX**	**Dimen-sions**	**Design air-to-refrigerant HEX (other parameter)**	**Dimensions internal air HEX**	**Dimen-sions external air HEX**
Number of plates	200	Tube outer diameter	1 inch	Number of tube rows	15	12
Plate length	12 m	External area of bundle face area	26.8 m^2/m^2	Total external area (APSF)	402 m^2/m^2	321.6 m^2/m^2
Plate width	4 m	APF	m^2/m tube	Height (y-axis to flow)	4.5 m	2 m
Plate distance	8 cm	Fin height	1.59 cm	Width (x-axis to flow)	2 m	10 m
Plate thickness	2 cm	Fins per meter	394	Face area	9 m^2	20 m^2
Total flow area	3.2 m^2	Wall thickness	1.5 mm	Finned tube area	3,618 m^2	6,432

Total HEX area	9,600 m^2	Flow area per tube	3.94 cm^2	Number of tubes	1,064	378
Width of HEX	2 m	Tube inner radius	1.12 cm	Length (z-axis to flow)	1.28 m	1.03 m

3.2 Calculations for the heating, ventilation and air conditioning system (HVAC)

General heat exchanger (HEX) equations:

Equations S89 to S98 are general equations used in heat exchanger calculations.

$$A_{fch} = W_{plate} * D_{plate} \quad \textit{Eq. S89}$$

$$u_{air,a2a,int} = \frac{V_{air,hvac}}{\frac{N_{plate}}{2} * A_{fch}} * f_{a2a,share} \quad \textit{Eq. S90}$$

$$D_{hyd} = \frac{4 * A_{fch}}{2 * (W_{plate} + D_{plate})} \quad \textit{Eq. S91}$$

$$F_{air,a2a,ext} = u_{air,a2a,ext} * \rho_{air,outside} * A_{fch} * \frac{N_{plate}}{2} \quad \textit{Eq. S92}$$

$$A_{hex,a2a} = N_{plate} * L_{plate} * W_{plate} \quad \textit{Eq. S93}$$

Note: Equations from http://www.heattransferconsult.nl/Tradi_Plate_Calc.html

$$Re = \frac{D * u_{air} * \rho_{air}}{\mu_{air}} \quad \textit{Eq. S94}$$

$$Pr = \frac{\nu_{air}}{a_{air}} \quad \textit{Eq. S95}$$

$$Nu = 0.023 * Re^{0.8} * Pr^{0.33} \quad \textit{Eq. S96}$$

$$\alpha = \frac{Nu * \lambda_{air}}{D} \quad \textit{Eq. S97}$$

$$U_{hex} = \frac{1}{\frac{1}{\alpha_{int}} + \frac{1}{\alpha_{ext}} + \frac{L}{\lambda_{tube}}} \quad \textit{Eq. S98}$$

Note: From [9], D is either $D_{hex,equiv}$ or D_{hyd}.

The dynamic and kinematic viscosity, thermal diffusivity and conductivity, as well as the density of the air were found to differ significantly across the temperature range considered in this work (-20 °C to plus 40 °C). Therefore, temperature (in Celcius) dependent terms were derived for this work to increase accuracy (equations S99 to S103).

$$\mu_{air} = 5 * 10^{-8} * T + 2 * 10^{-5} \quad \textit{Eq. S99}$$

$$\rho_{air} = -0.0046 * T + 1.2978 \quad \textit{Eq. S100}$$

$$\nu_{air} = 9 * 10^{-8} * T + 1 * 10^{-5} \quad \textit{Eq. S101}$$

$$a_{air} = 1 * 10^{-7} + 2 * 10^{-5} \quad \textit{Eq. S102}$$

$$\lambda_{air} = 8 * 10^{-5} * T + 0.0241 \quad \text{Eq. S103}$$

Source: https://www.me.psu.edu/cimbala/me433/Links/Table_A_9_CC_Properties_of_Air.pdf

NTU method for counter flow plate HEX:

Source for NTU method: [35]

$$F_{air,a2a,int} = F_{hvac} * f_{a2a,share} \quad \text{Eq. S104}$$

$$C_{air,ext} = F_{air,a2a,ext} * C_{p,air} \quad \text{Eq. S105}$$

$$C_{air,int,1} = F_{air,a2a,int} * C_{p,air} \quad \text{Eq. S106}$$

$$C_{min,1} = MIN(C_{air,ext}, C_{air,int,1}) \quad \text{Eq. S107}$$

$$C_r = \frac{C_{min}}{C_{max}} \quad \text{Eq. S108}$$

Note: Cr and ϵ were calculated for both the cooling-only case (1) and the cooling and condensation case (23).

$$NTU_1 = \frac{U_{hex,a2a} * A_{hex,a2a} * f_{cooling\ ratio}}{C_{min,1}} \quad \text{Eq. S109}$$

Note: Here, the cooling ratio $f_{cooling\ ratio}$ is introduced, taking initially the value 1.

$$\epsilon = \frac{1 - e^{-NTU*(1-C_r)}}{1 - C_r * e^{-NTU*(1-C_r)}} \quad \text{Eq. S110}$$

$$Q_{1,max} = \left(T_{air,hvac,in} - T_{air,outside}\right) * C_{min,1} \quad \text{Eq. S111}$$

$$Q_{1,pot} = \epsilon * Q_{1,max} \quad \text{Eq. S112}$$

$$Q_{1,req} = \begin{cases} \left(T_{air.hvac,in} - T_{air,hvac,out}\right) * C_{air,int,1} & if\ m_{w,out} = 0 \\ \left(T_{air.hvac,in} - T_{condens}\right) * C_{air,int,1} & else \end{cases} \quad \text{Eq. S113}$$

$$Q_{1,actual} = MIN(Q_{1,req}, Q_{1,pot}) \quad \text{Eq. S114}$$

Note: $Q_{1,req}$ is the share of cooling required to decrease the temperature until T = T_{sat}, i.e. $T_{condens}$ at which condensation occurs

$$f_{cooling\ ratio} = \frac{Q_{1,req}}{Q_{1,pot}} \quad \text{Eq. S115}$$

$$C_{air,int,23} = F_{air,a2a,int} * \frac{\Delta h}{\Delta T} \quad \text{Eq. S116}$$

Note: This is now the NTU method applied to the section of the HEX which cools and condenses simultaneously (indicated by the suffix 23), requiring an approximation of the C value.

$$\frac{\Delta h}{\Delta T} = \frac{(0.0626 * T_{condens}^2 + 0.9943 * T_{condens} + 12.771) - \left(0.0626 * T_{equiv}^2 + 0.9943 * T_{equiv} + 12.771\right)}{T_{condens} - T_{equiv}} \quad \text{Eq. S117}$$

$$C_{min,23} = MIN(C_{air,ext}, C_{air,int,23}) \quad \textit{Eq. S118}$$

Note: The polynomial equation was obtained from plotting the enthalpy of saturated air vs its saturation temperature

$$NTU_{2,3} = \frac{U_{hex,a2a} * A_{hex,a2a} * (1 - f_{cooling\ ratio})}{C_{min,23}} \quad \textit{Eq. S119}$$

$$Q_{23,req} = Q_{cool,req} - Q_{1,req} \quad \textit{Eq. S120}$$

$$Q_{23,max} = \left(T_{air,ext,in} - T_{condens}\right) * C_{min,23} \quad \textit{Eq. S121}$$

$$Q_{23,pot} = MIN(\epsilon * Q_{23,max}, Q_{23,req}) \quad \textit{Eq. S122}$$

Note: Epsilon in this equation is recalculated from C_r with $C_{air,int,cond}$ and $NTU_{2,3}$

$$T_{air,ext,post-cond} = T_{air,ext,in} + \frac{Q_{23,pot}}{C_{air,ext}} \quad \textit{Eq. S123}$$

Note: This calculates the estimated temperature of the outside air at the end of the air-to-air heat exchanger section which is cooling and condensing, i.e. just before the cooling-only section. This is relevant in a counter-flow heat exchanger and the estimated temperature value is then used again to reassess the duty of the cooling-only duty Q_1.

$$T_{air,int,post-cond} = T_{condens} - \frac{Q_{23,pot}}{C_{air,int,23}} \quad \textit{Eq. S124}$$

$$Q_{max,1,check} = \left(T_{int,hvac,in} - T_{air,ext,post-cond}\right) * C_{min,1} \quad \textit{Eq. S125}$$

$$Q_{1,est} = \epsilon * Q_{max,1,check} \quad \textit{Eq. S126}$$

Note: ϵ was recalculated here from C_r with $C_{air,int,cool}$ and NTU_1 with $f_{cooling\ ratio,new}$

$$Error = \frac{MAX\left(Q_{1,actual}, Q_{1,est}\right) - MIN\left(Q_{1,actual}, Q_{1,est}\right)}{Q_{1,actual}} \quad \textit{Eq. S127}$$

$$f_{cooling\ ratio,new} = \begin{cases} \dfrac{f_{cooling\ ratio,old}}{1 + Error} & if\ Q_{1,est} > Q_{1,actual} \\ 1 - \dfrac{1 - f_{cooling\ ratio,old}}{1 + Error * 2} & else \end{cases} \quad \textit{Eq. S128}$$

Note: The 2 was added in the denominator as it was found that when the initial ratio results in a low $Q_{1,est}$, 4 iterations were not enough to get it close to $Q_{1,actual}$. After this step, NTU_{23}, ϵ_{23}, $Q_{23,pot}$, $T_{air,ext,post-cond}$, $T_{air,int,post-cond}$, NTU_1, ϵ_1, $Q_{max,1,check}$, $Q_{1,est}$and $Error$ are calculated again to obtain a new cooling ratio. Four Iterations of this have been carried out to reach $f_{cooling\ ratio,final}$.

$$Q_{23,final} = MIN(Q_{23,pot} + \left(Q_{1,est} - Q_{1,actual}\right), Q_{23,req}, Q_{23,max}) \quad \textit{Eq. S129}$$

Note: Based on $Q_{23,final}$, the final $T_{air,ext,post-cond}$, $T_{air,int,post-cond}$ are calculated and used to calculate the LMTD for a feasibility check

$$LMTD_{23,check} = \frac{\left(T_{air,int,post-cond} - T_{air,outside}\right) - \left(T_{condens} - T_{air,ext,post-cond}\right)}{LN\left(\frac{T_{air,int,post-cond} - T_{air,outside}}{T_{condens} - T_{air,ext,post-cond}}\right)} \quad \text{Eq. S130}$$

$$Q_{23,check} = U_{hex,a2a} * A_{a2a} * \left(1 - f_{cooling\ ratio,final}\right) * LMTD_{23,check} \quad \text{Eq. S131}$$

$$Q_{23,actual} = MIN(Q_{23,final}, Q_{23,check}) \quad \text{Eq. S132}$$

$$Q_{cool,remain,a2a} = Q_{cool,req} - Q_{1,actual} - Q_{23,actual} \quad \text{Eq. S133}$$

$$T_{air,int,a2a,out} = \begin{cases} T_{air,int,post-cond} & if\ Q_{23,actual} > 0 \\ T_{air,hvac,in} - \frac{Q_{1,actual}}{C_{air,int,cool}} & if\ Q_{23,actual} = 0 \\ T_{air,hvac,in} & if\ F_{air,int} = 0 \end{cases} \quad \text{Eq. S134}$$

$$\Delta P_{plate} = f_D * \frac{\rho_{air}}{2} * \frac{u_{air,a2a}^2}{D_{plate}} * L_{plate} \quad \text{Eq. S135}$$

$$f_D = \frac{0.25}{\left(\log_{10}\left(\frac{\epsilon_{surface}}{3.7 * D_{hyd}} + \frac{5.74}{Re^{0.9}}\right)\right)^2} \quad \text{Eq. S136}$$

Note: Darcy Weisbach equation, Darcy friction factor according to [39]. Pressure drop was calculated for both internal and external air flow.

$$E_{fans,a2a,int} = V_{hvac} * f_{a2a,share} * \Delta P_{plate,int} * \frac{1}{\eta_{fans}} \quad \text{Eq. S137}$$

$$E_{fans,a2a,ext} = F_{air,ext} * \rho_{air,outside} * \Delta P_{plate,ext} * \frac{1}{\eta_{fans}} \quad \text{Eq. S138}$$

Refrigeration cycle and compressor

The methodology to calculate the electricity consumption of the refrigeration cycle and the air-source heat pump (both including compressor, process side air fan and exterior air fan) is based on [9] and expanded with variable condenser and evaporator temperatures, polynomial equations for the state variables, and potential heat recovery to the process air. The P-h diagram of R134A and the saturated property table have been used to determine the COP of the compressor, the refrigerant flow and the cooling requirements of the refrigerant ($Q_{ref,cool}$) depending on T_{equiv}, $T_{hvac,out}$ and $T_{outside}$. Those have been combined with F_{hvac}, $Q_{cool,remain,a2a}$ and $Q_{heat,req}$ to determine the electricity consumption of compressor and fans. Heat recovery was incorporated by allowing the refrigerant in the refrigeration cycle to cover a part of its cooling requirement by flowing through the HEX of the condenser within the heat pump cycle (when the heat pump was off, assuming the same refrigerant).

$$T_{1s} = \begin{cases} T_{air,equiv} - \Delta T_{evap} & m_{w,out} > 0 \\ T_{hvac,out} - \Delta T_{evap} & else \end{cases} \quad \text{Eq. S139}$$

$$T_{3s} = \begin{cases} T_{outside} + \Delta T_{cond,outside} & if\ T_{outside} + \Delta T_{cond,outside} > T_{hvac,out} + \Delta T_{cond,inside} \\ T_{hvac,out} + \Delta T_{cond,inside} & if\ T_{hvac,out} + \Delta T_{cond,inside} > T_{1,s} + \Delta T_{cond,inside}\ , m_{w,out} > 0 \\ T_{1,s} + \Delta T_{cond,inside} & else \end{cases} \quad \text{Eq. S140}$$

Note: This equation ensures that the condenser temperature is always above the evaporator temperature, while also ensuring that reheating (heat transfer from the compressed refrigerant to the internal air post-condensation) is feasible

without unnecessarily increasing the required compressor input. The equation changes slightly for the cooling-only case (no reheating required):

$$T_{3s} = \begin{cases} T_{outside} + \Delta T_{cond,outside} & if\ T_{outside} + \Delta T_{cond,outside} > T_{1,s} + \Delta T_{cond,inside}\ , m_{w,out} > 0 \\ T_{1,s} + \Delta T_{cond,inside} & else \end{cases} \quad \text{Eq. S141}$$

The other conditions at the respective stages in the refrigeration cycle are described by equations S142 to S153.

$$T_1 = T_{1s} + \Delta T_{sup} \quad \text{Eq. S142}$$

$$T_3 = T_{3s} - \Delta T_{sub} \quad \text{Eq. S143}$$

$$h_{1s} = h_{ref,sat\ vap}@T_{1s} = -0.0014 * {T_{1s}}^2 + 0.5722 * T_{1s} + 250.53 \quad \text{Eq. S144}$$

$$h_{sat,cond} = h_{ref,sat\ vap}@T_{3s} = -0.0014 * {T_{3s}}^2 + 0.5722 * T_{3s} + 250.53 \quad \text{Eq. S145}$$

$$h_1 = h_{1s} + C_{p,vapour} * (T_1 - T_{1s}) \quad \text{Eq. S146}$$

$$h_{3s} = h_4 = h_{ref,sat\ liq}\ @T_{3s} = 0.0016 * {T_{3s}}^2 + 1.3504 * T_{3s} + 51.816 \quad \text{Eq. S147}$$

$$h_3 = h_{3s} + C_{p,liquid} * (T_3 - T_{3s}) \quad \text{Eq. S148}$$

$$s_{1s} = s_{ref,sat\ vap}@T_{1s} = -0.00000009 * {T_{1s}}^3 + 0.000007 * {T_{1s}}^2 - 0.0005 * T_{1s} + 0.9313 \quad \text{Eq. S149}$$

$$s_1 = s_{1s} + \frac{(h_1 - h_{1s})}{dh/ds} \quad \text{Eq. S150}$$

$$s_{sat,cond} = s_{ref,sat\ vap}\ @T_{3s} = -0.00000009 * {T_{3s}}^3 + 0.000007 * {T_{3s}}^2 - 0.0005 * T_{3s} + 0.9313 \quad \text{Eq. S151}$$

$$h_{2s} = h_{sat,cond} + \frac{dh}{ds} * (s_1 - s_{sat,cond}) \quad \text{Eq. S152}$$

$$h_2 = \frac{h_{2s} - h_{1s}}{0.8} + h_{1s} \quad \text{Eq. S153}$$

Note: The 2nd order polynomial equations for enthalpy (3rd order for entropy) were derived from the saturated property table of refrigerant R134A.

$$COP_{comp} = \frac{h_1 - h_4}{h_2 - h_1} \quad \text{Eq. S154}$$

$$E_{comp,ref} = \frac{Q_{cool,remain,a2a}}{COP} \quad \text{Eq. S155}$$

Note: This is the electricity consumption of the compressor required to perform the cooling duty remaining after the air-to-air HEX.

$$m_{R134A,ref} = \frac{Q_{cool,remain,a2a}}{h_1 - h_4} \quad \text{Eq. S156}$$

$$LMTD_{ref} = \frac{\left(T_{air,int,a2a,out} - T_{1s}\right) - \Delta T_{evap}}{LN\left(\frac{T_{air,int,a2a,out} - T_{1s}}{\Delta T_{evap}}\right)} \quad \text{Eq. S157}$$

$$u_{air,int,ref} = \frac{V_{hvac}}{A_{face,ref,int}} \quad \text{Eq. S158}$$

The process air side variables (Re, Nu, α, U-value) were calculated as shown earlier (using $D_{hex,equiv}$) and used in the below equation.

$$Q_{ref,pot} = U_{hex,ref} * A_{hex,ref,int} * LMTD_{ref} \quad \text{Eq. S159}$$

Note: This equation was used to size the heat exchanger to ensure the required cooling loads can be realised

The process side air pressure drop and fan power consumption ($E_{fan,ref,int}$) was calculated as described in https://cheguide.com/air_cooled_exch.html using the finned tube and HEX geometry (face area and face mass velocity) to obtain static and kinetic pressure drop [40–43]. The dimensions are indicated in the parameter table for both the process air to refrigerant HEX and the outside air to refrigerant HEX. If the complete cooling duty was realised in the air-to-air HEX, fan power consumption of the refrigeration cycle was assumed to be zero as it would be bypassed.

Heat recovery, air cooling of refrigerant and air-source heat pump reheating

The refrigerant has absorbed heat in the evaporator and through the compressor input. This now needs to be rejected, either back to the internal air stream for reheating after condensation (recovery), or to outside air. If reheating does not take place or only partially covers the heating requirement, additional heat needs to be supplied by the ASHP.

$$Q_{R134A,cool} = m_{R134A,ref} * (h_2 - h_3) \quad \text{Eq. S160}$$

$$LMTD_{recovery} = \frac{(T_{equiv} - T_{sat,cond}) - (T_{sat,cond} - T_{hvac,out})}{LN\left(\frac{T_{equiv} - T_{sat,cond}}{T_{sat,cond} - T_{hvac,out}}\right)} \quad \text{Eq. S161}$$

$$Q_{recovery,pot} = U_{hex,ref} * A_{hex,ref,int} * LMTD_{recovery} \quad \text{Eq. S162}$$

$$Q_{recovery,actual} = MIN(Q_{recovery,pot}, Q_{heat,req}, Q_{R134A,cool}) \quad \text{Eq. S163}$$

$$Q_{heat,ASHP} = Q_{heat,req} - Q_{recovery,actual} \quad \text{Eq. S164}$$

$$Q_{R134A,remain} = Q_{R134A,cool} - Q_{recovery,actual} \quad \text{Eq. S165}$$

$$T_{outside,out,max} = T_{sat,cond} - \Delta T_{min,R134a,air} \quad \text{Eq. S166}$$

$$F_{air,cond,req} = \frac{Q_{R134A,remain}}{(T_{outside,out,max} - T_{air,outside}) * C_{p,air}} \quad \text{Eq. S167}$$

$$u_{air,cond} = \frac{F_{air,cond,req}}{\rho_{outside} * A_{face,ref,ext}} \quad \text{Eq. S168}$$

The outside air pressure drop and fan power consumption ($E_{fan,ref,ext}$) was calculated as shown in https://cheguide.com/air_cooled_exch.html with the dimensions indicated in the fixed parameter table for the refrigerant to outside air HEX and $u_{air,cond}$.

$$E_{fans,a2a} = E_{fan,a2a,int} + E_{fan,a2a,ext} \quad \text{Eq. S169}$$

$$E_{RC} = E_{comp,ref} + E_{fan,ref,int} + E_{fan,ref,ext} \quad \text{Eq. S170}$$

The electricity consumption of the compressor and the fan for the refrigerant to outside air HEX was based on an equation generated from empirical data [44].

$$COP_{ASHP} = 6.7 * e^{-0.022*(T_{air,hvac,out}+15-T_{air,outside})} \quad \text{Eq. S171}$$

$$E_{ASHP} = \frac{Q_{heat,ASHP}}{COP_{ASHP}} \quad \text{Eq. S172}$$

$$COP_{cool,LED} = 25.067 * e^{0.05*T_{outside}} \quad \text{Eq. S173}$$

Source: From plotted data relating the outside temperature to the compressor and air cooling fan power with fixed refrigerant temperatures (20 C inlet and 45 C outlet), assuming the same condenser and evaporator settings as describes for the process air heat exchangers in this section, independent of duty. The maximum feasible COP was limited to 20.

$$E_{cool,LED} = \frac{Q_{cool,LED}}{COP_{cool,LED}} \quad \text{Eq. S174}$$

4 Model parameter

4.1 Evapotranspiration

Several physical and empirical models have been proposed which aim to correlate the transpiration rate of plants to measurable parameters in the greenhouse [29]. It seems that all of those models result in some over- or underestimation compared with experimental data, in particular when considering early plant stages, different crops or parameters close to zero [13,45]. In this study, the model by Graamans et al. [17] was selected due to its ease of application with climate and crop variables obtainable or determinable from commonly available data (equations S175 to S 179). A topic of debate is the calculation of the r_s value, the stomatal resistance [13]. We found that all of the proposed relations showed significant over- or underestimation for conditions at which the model was not validated, such as high VPD, very low radiation or low air velocities typically found in PF. We thus defined the terms in the r_s equation (equation S180) empirically by minimising the error for two sets of experimentally obtained ET values with known conditions [30,46]. The CO_2 term was taken from Stanghellini (1987), the temperature term was dropped as it is both very plant-specific and excluded in most models due to its interrelation with other parameters, e.g. VPD [29]. The VPD term was the most sensitive one, and a linear relation resulted in the smallest deviation from measurements and reflected the ET vs VPD curves from experimental studies [45,46]. The hyperbolic VPD term leads to very large r_s values at higher VPD values (above 1 kPa, outside the applicability range reported in [47]), which would lead to a drop in evapotranspiration rates at higher VPD values, something not observed in the previously mentioned studies for plant factories or for plants in general [48]. The small values of the radiation terms C1 and C2 suggested by other works result in a sharp drop of the overall radiation term of 1 at very low light levels [47] and could thus not represent measurements taken at those conditions. The terms used in Graamans et al. [17] make it less sensitive but were also empirically determined for a specific set of measurements not covering all ranges. Since we used watts instead of photosynthetic photon flux density in this work, we adjusted $r_{s,min}$, C1 and C2 values from curve fitting and least deviation from measurements. Finally, ET was equated to ET0, as suggested by crop coefficients close to 1 [46].

$$I_{net} - LH - SH = 0 \quad \text{Eq. S175}$$

$$ET = \frac{LH}{\lambda_{leaf}} * \frac{3600\frac{s}{h}}{1000\frac{J}{kJ}} \quad \text{Eq. S176}$$

$$LH = LAI * \lambda_{leaf} * \frac{VCD}{r_s + r_a} \quad \text{Eq. S177}$$

$$SH = \rho_{center} * C_{p,air} * LAI * \frac{T_{leaf} - T_{air,center}}{r_a} \quad \text{Eq. S178}$$

$$r_a = 350 * \left(\frac{D_{leaves}}{u_{air,center}}\right)^{0.5} * \frac{1}{LAI} \quad \text{Eq. S179}$$

$$r_c = \begin{cases} r_{s,min} * \frac{I_{net,PAR} + C_1}{I_{net,PAR} + C_2} * \left(1 + C_3 * \frac{VPD_{leaf}}{10}\right) * (1 + C_4 * (CO_2 - 200)^2) * \frac{1}{2} & if\ I_{net} > 0 \\ r_{s,min} * \frac{C_1}{C_2} * \left(1 + C_3 * \frac{VPD_{leaf}}{10}\right) * \frac{1}{2} & else \end{cases} \quad \text{Eq. S180}$$

$$Q_{SH} = SH * A_{growing} \quad \text{Eq. S181}$$

Sources: [29,30,47]

4.2 Crop growth and yield

The yield-light dependency was chosen from Graamans et al. [7] and Van Henten [18]; doubling the DLI output increases the crop growth by a factor of 1.74 for all crops, similar to findings from other experiments [49,50]. The target DLI determined the whitewash (light, 25% reduction or strong, 50% reduction) for the GHs as described in S1.3. This more rigid control of solar radiation in GHs (as opposed to flexible shading screens for example) meant that for months which did not require additional lighting in GHs, slightly more PAR than the target DLI was received by the plants. This was accounted for by adjusting the yield according to equation S182.

$$YF_{correction} = \left(\frac{DLI_{actual}}{DLI_{target}} - 1\right) * 0.74 + 1 \quad \text{Eq. S182}$$

The yield-CO_2 dependency (equation S183) was chosen from [34] as it is in line with results from other works [2,51]. The yield-temperature dependency equation (S184) was chosen from Li et al. [34] and maximum temperatures were adjusted (between indicated value and 40 C) to reflect the possibility to obtain adequate yields for certain crops above the indicated temperatures [7].

$$YF_{CO2} = \frac{1 - e^{-0.003} * (CO2_{centre} - 56)}{1 - e^{-0.003} * (CO2_{ref} - 56)} \quad \text{Eq. S183}$$

$$YF_T = \frac{T_{max} - T_{air}}{T_{max} - T_{opt}} * \left(\frac{T_{air}}{T_{opt}}\right)^{\frac{T_{opt}}{T_{max} - T_{opt}}} \quad \text{Eq. S184}$$

$$YF_{total} = YF_{CO2} * \left(\frac{YF_{T,center} * 4 + YF_{T,GH_{in}} + YF_{T,GH_{out}}}{6}\right) * YF_{rad} * YF_{correction} \quad \text{Eq. S185}$$

Since a temperature gradient exists within the structure with the more optimum temperature in the centre, an approximation of the integral was carried out to account for this (equation S185).

Note: in the PF and CGH, the suffix *GH,in* becomes *hvac,out* and *GH,out* becomes *hvac,in*. The temperature yield factor differs between the locations in the greenhouse and is represented by a sin-curve, hence an approximation of the integral is used in this equation.

4.3 Duration and timing of photoperiod

The length of the photoperiod in GH was assumed to be at least 12 hours, from 7 AM to 7 PM, and longer for summer days when the solar radiation in a given hour before 7 AM or after 7 PM was above 50 W/m^2. This ensured minimum energy requirements for cooling when the sunhours are longer. The length of the PF was adjusted to the recommended photoperiod for each crop [52] and and thus the vegetable basket proxy. The daily yield was divided by the length of the photoperiod in hours to obtain the hourly yield. Moreover, the photoperiod in PF is considered to be at night to reduce cooling costs associated with waste heat from artificial lighting [7]. The slightly higher duration of the photoperiod in the PF is assumed to not negatively affect the yield but helps to distribute the cooling load for the PF.

4.4 Crop properties and parameter table

The theoretical optimum and maximum temperature range values in table S2 for tomatoes, bell peppers, broccoli and zucchini were obtained from [34] and growers' recommendations. The minimum and maximum temperatures to be realised during the different periods by growers as described in SI 4.2 are also shown in table S2 below.

The photoperiod, reference yield at 800 ppm CO_2 (using the harvest index) and default DLI values were selected for bell pepper [52,53], lettuce, spinach, broccoli [34,52], zucchini (www.greenhousegrower.com/production/zucchini-in-the-greenhouse/) and tomato [54,55] with slight adjustments based on LED suppliers' recommendations (www.horti-growlight.com/typical-ppfd-dli-values-per-crop).

To the authors' knowledge, there has so far been no attempt to produce statistically significant information on achievable yields at certain DLI levels and fixed conditions (e.g. temperature, VPD). Hence, these values reflect the authors best attempt to consolidate multiple sources and sometimes incongruent information (e.g. the tomato yield at a given DLI ranged from 30 kg/m2 at 25.9 mol/day [8] to 74 kg/m2 at 20 mol/day [54]). They serve here as a basis for the modelling effort and might differ in practice and between cultivars. The LAI was assumed to be constant for each crop given the different growth stages present in typical GH and PF; 2.1 for lettuce [7], 2.8 for tomato [54] and 2.5 for the basket.

Table S2: Composition of the vegetable basket and properties of the crops considered in it

Crop	Share in basket	Photoperiod PF (h)	Reference yield (kg m^{-2} $year^{-1}$)	Default DLI (mol day^{-1})	T_{opt}, T_{max} (C)	T_{min}, T_{max} (photo, C)	T_{min}, T_{max} (night, C)
Lettuce	12%	16	52.6	11.5	18, 33.5	11.6, 24.1	6, 14
Tomato	40%	12	56.0	16	27, 40	20.6, 32.5	15, 23
Broccoli	12%	16	18.1	12.4	16, 29	10.5, 21.2	4, 12
Bell pepper	12%	12	16.6	15	24, 38.5	17.3, 30	12, 20
Spinach	12%	16	27.8	10.7	18, 36	11, 25	6, 14
Zucchini	12%	16	8.5	10.8	18, 35	11.3, 24.6	6, 14
Vegetable basket	-	14	38.0	13.7	22.1, 36.6	15.6, 28.0	10.1, 18.1

5 Exterior climate

5.1 Latitude and sun-hours

The latitude is an indicator of the daily hours of sunshine, depending on the day of the year. Third order polynomial equations were developed which relate the latitude to the average daily sun hours for a given month. Data was obtained from https://www.engr.scu.edu/~emaurer/tools/calc_solar_cgi.pl. The coefficients are listed in table S3 below, equations were of the form $sun\ hours = a * x^3 + b * x^2 + c * x * d$, with x being the latitude.

Table S3: Coefficients of the third order polynomial equation used to relate latitude to the sunhours at the 15th day of the respective month.

Month	First coefficient (a)	Second coefficient (b)	Third coefficient (c)	Fourth coefficient (d)
January	-2.00E-05	-4.00E-05	-0.0381	12.043
February	-8.00E-06	-3.00E-05	-0.0262	12.023
March	-2.00E-06	-8.00E-06	-0.0054	12.006
April	5.00E-06	1.00E-05	0.0173	11.988
May	1.00E-05	6.00E-05	0.0348	11.955

Field Code Changed
Field Code Changed
Formatted: English (United Kingdom)
Formatted: English (United Kingdom)
Field Code Changed

June	2.00E-05	0.0001	0.0361	11.924
July	2.00E-05	9.00E-05	0.0377	11.953
August	9.00E-06	3.00E-05	0.0261	11.973
September	1.00E-06	1.00E-06	0.0056	11.998
October	-6.00E-06	-2.00E-05	-0.0167	12.018
November	-1.00E-05	-5.00E-05	-0.0338	12.043
December	-2.00E-05	-1.00E-04	-0.0361	12.076

5.2 Extraction of climate data for the metropolitan regions

The local values were aggregated to an average for each region and an attempt was made to ensure the regions are roughly similar in size. The administrative boundaries were either country (level 1), state (level 2) or county (level 3). Each country defines their administrative boundaries differently (e.g. in some cases the county level is the municipal level while in other cases states are called regions or prefectures), so for easier comparison the definition by GADM was used here (https://gadm.org/download_world.html). The monthly temperature (min, max), water vapour pressure and solar radiation (daily average total) values were extracted from https://www.worldclim.org/.

The climate data was obtained as a raster file and extracted for the centre point of the regions indicated in the table below. The steps in ArcGIS were:

1. Merge selected administrative polygons
2. Feature to Point
3. Extract Multi values to points (5*12 values for each region)

5.3 Selection of regions

Table S4: List of regions and their climatic properties used in this study

Name of the region	Administrative type (level)	Average DLI natural (PAR, mol/(m2* day))	Mean annual temperature (C)	Climate zone (Köppen climate zone classification)	Latitude
Reykjavik region (Iceland)	Counties (3)	15.40	4.7	Cfc / ET	64.15 N
Stockholm region (Sweden)	States (2)	19.69	7.0	Cfb	59.46 N
Tokyo region (Japan)	States (2)	26.17	15.6	Cfa	35.51 N
Massachusetts (US)	State (2)	26.46	9.8	Cfa / Dfb	42.26 N
Tasmania (Australia)	State (2)	27.96	12.4	Cfb	41.97 S
Singapore	Country (1)	32.49	26.8	Af	1.35 N
Santiago region (Chile)	States (2)	33.71	14.6	Csb	33.59 S
Maricopa county (Arizona, US)	County (3)	39.73	21.94	Bwh	33 N
Gauteng (South Africa)	State (2)	40.35	16.0	Cwb	26.11 S
United Arab Emirates	Country (1)	42.83	26.7	Bwh	23.91 N

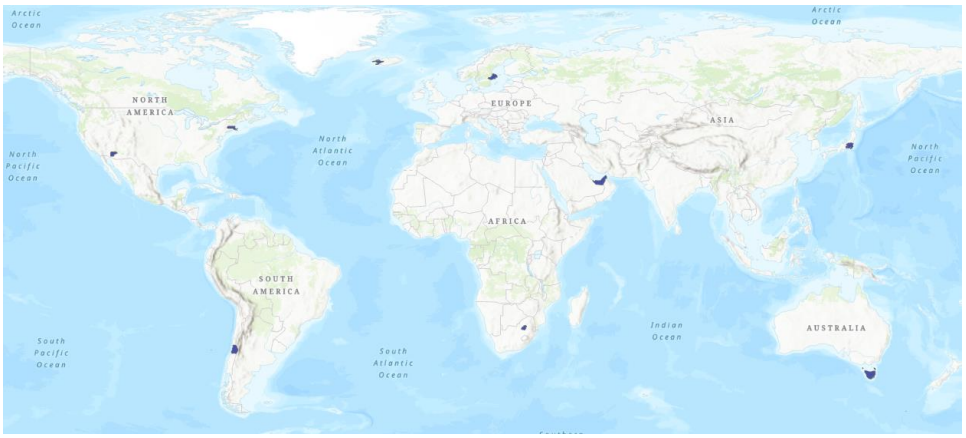

Figure S7: Location of the regions on the globe considered in this study. Note: Singapore is hardly visible

6 Optimisation routine

The optimisation was carried out with a Solver macro in Excel to facilitate the selection of different locations, crops and settings. This made it necessary to split the optimisation in two steps (specific energy and evapotranspiration balance), using multiple loops with convergence to update the conditions at the centre of the facility. The optimisation was finished when venting and HVAC flowrate, temperature and VPD would not change more than 2.5%, usually achieved within four iterations (10-30 seconds per hourly optimisation). The GRG non-linear engine was used with a convergence of 0.001.

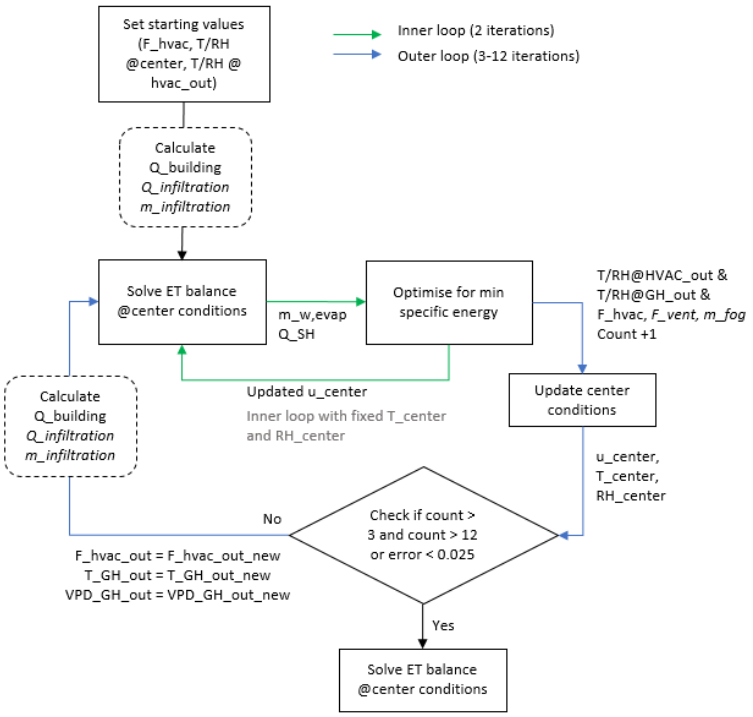

Figure S8: Schematic of the optimisation routine as constructed in Excel VBA

$$\text{Error} = \frac{\frac{(F_{hvac,new} - F_{hvac})}{F_{hvac}} + \frac{(T_{hvac,out,new} - T_{hvac,out})}{T_{hvac,out}} + \frac{(VPD_{hvac,out,new} - VPD_{hvac,out})}{VPD_{hvac,out}}}{3}$$

7 Scenario analysis

Besides the choice of crop, a range of other parameters also has a considerable influence on the results. Table S5 shows these scenarios, listed by assumptions, design variables and control variables. Some of those parameters and the decisions taken are explained below.

Table S5: Overview of the 18 scenarios used in the parametric sensitivity analysis

Category	#	Aspect	Standard value	Scenario analysis
Physical behaviour assumptions	1	Minimum stomatal resistance	60	82
	2	Permissible VPD range	4 tp 12 kPa	6 to 10 kPa
	3	LED efficiency	59%	75%

	4	U-value of the cover	GH: 2 (ETFE) and 2.27 (PC), PF: 0.3	Twice as much
	5	Permissible temperature differences in the refrigeration cycle	ΔTcond = 15 ΔTevap = 8	ΔTcond = 8 ΔTevap = 5
Design variables	6	Building size	Volume fixed	Half the floor area
	7	Geometry	Rectangular (W/L=0.5)	Square (W/L=1)
	8	Size of heat exchangers	See table S1	Half as much area
	9	Target DLI	13.7 mol/(m^2*day)	Twice as much
	10	CO2 supply intensity	0.3 kg CO_2/kg yield	No limit (PF only)
	11	Crop	Basket	Lettuce
	12, 13	Climate preference	Mild	Warm, Cold
Control variables	14	LED water cooling	Variable (GHs only)	Off
	15	LED dimming (GHs only)	To compensate low sunshine in the morning and afternoon (GHs only)	Fixed power (250 µmol/m^2/s)
	16	Optimised parameter	Specific energy	Energy consumption only
	17	Air-to-air cooling	Variable bypass	Off
	18	Variable LED cooling	Variable (GHs only)	Fixed on
	19	Yield optimisation	Minimisation of hourly specific energy	Maximisation of hourly yield

Geometry

Since the greenhouse is East-West oriented, the geometry determines the length of the sturdy wall not facing the sun (North for above the equator and South for below) and thus indirectly the overall U-value and the design of the AHU. The standard value is width / length = 0.5. Results are also obtained for W/L = 1, essentially a square. Further, the size of the building is doubled in one of the scenarios.

LED efficiency

The efficiency of LEDs has increased over the last year and further technological advancement cause this trend likely to continue [56]. The sensitivity of the results due to LED efficiency and the comparative benefit to GH and PF is assessed with an efficiency value of 75% or 3.5 µmol/J (https://www.horti-growlight.com/coolpack-horti-led-top-light).

U-value of walls

The overall heat transfer coefficient describes the possible heat exchange driven by a difference in temperature between inside and outside air. In continental and colder climate zones, winter heating is a significant contributor to the annual heating requirements [57]. The choice of ethylene tetrafluoroethylene film is thus justified from an energy perspective. However, it might not be realisable in every circumstance, e.g. due to the availability of equipment required to install it. Moreover, some plant factories might be situated in very well-insulated buildings. To assess the effect of the U-value and thus the wall material on the total energy consumption, results are also obtained for a U-value of 0.05 W/(m^2*C) for PF and twice the U-value for PC (2*2.27 W(m^2*C)) and ETFE (2*2 W(m^2*C)).

Light intensity

Increasing the moles of PAR received per day comes with diminishing returns for higher light levels [2]. Considering that artificial lighting is the primary electricity consumer in PF [7] and GH in less sunny climates [20], balancing the light supplied with the power consumption is a way to increase profits by reducing the cost per kg of crop produced [33]. The reference yield values were obtained at the indicated Default DLI which for lettuce can be equated with 16 hours of 250 µmol/(m^2*s). This was assumed to be common practice and thus chosen for the default case while a doubling of the light intensity (for lettuce 500 µmol/(m^2*s) and thus the DLI required was also assessed. Increasing the DLI much further than that was found to increase yield only marginally while almost linearly increasing the electricity consumption and was thus not selected.

CO_2 concentration in the air

The positive influence of CO_2 on crop growth is well known. However, some discrepancies exist for the effect on the photosynthesis rate of a higher CO_2 concentration between 1200 and 1600 ppm. Some models suggest that increasing the CO_2 concentration at higher light intensities has a more substantial effect on the yield compared with the same increase at lower light intensities [7,18], or similarly, that the photosynthesis rate reaches its maximum at lower CO_2 concentrations when the light intensity is lower [58]. Others suggest that the effect of increased CO_2 levels in the air is less dependent on the light intensity [2,34]. The photosynthesis rate increase calculated in one study [7] for switching the CO_2 concentration from 400 to 1600 ppm at 250 µmol m^{-2} s^{-1} (more than 3 times increased photosynthesis rate) could not be confirmed by reports from growers considering the actual yield of crops [59]. Hence, the simplified model from Li et al. [34] is employed for this work. Since CO_2 is contained with PF and CGH, a target CO_2 concentration of 1600 ppm is considered as the default and 400 ppm as an assessment of the influence on the comparative results between the growing practices.

Optimisation of specific energy and variable cooling

The operations of a climate-optimised greenhouse require a high level of sensors and automation in practice which not every grower desires or can afford. To test the influence on the specific energy obtained without such measures, the optimisation is carried out for a hypothetical "non-optimised" case in which a) LEDs are constantly fully water-cooled or have a constant light intensity during their active hours (GH-only), b) an air-to-air heat exchanger which can't be flexibly bypassed (either on or off) and c) the objective function during the day or photoperiod is the total electricity consumption (which would reduce controlling complexity). The latter means that the temperature limits are set to 85% of the maximum yield during the day and that the potential productivity loss due to venting (lower CO_2 levels) is ignored in the optimisation. Regarding the constant or non-dimmable light intensity of the LEDs, an output of 250 µmol/m^2/s was assumed and the required hours of operation calculated as described in SI 2.5. To compare this with the optimised versions, the effects on yield of the resulting climate are still considered and the specific energy is nevertheless chosen as the target indicator.

8 Assumptions and limitations

Growing facilities and space conditioning

- The airflow within the structure behaves similar to a plug flow reactor (PFR), with a uniform air velocity and changing its properties and composition along the length of the structure (gradient between inlet and outlet) while being the same along the width and height of the structure at a given length (perfect lateral mixing). Perfect lateral mixing might not be achieved with a typical ventilation system while increased flow above the canopy might lead to a lower gradient on the top compared with the bottom of the structure.
- Pressure drop within the structure on internal airflow (except on venting flow) is negligible
- The thermal storage effect of air is included but not that of walls, soil, and equipment. It was assumed that radiative and convective heat exchange between those and the air would balance itself out across the day and are thus negligible [1].
- All solar radiation entering the greenhouse (after cover reflection has been accounted for) stays at heat energy in the greenhouse, either a) absorbed by the plants and considered in the ET balance (ultimately transferred to the air

as latent and sensible heat), b) reflected from the plants into the air, c) reflected from the non-covered share of the growing beds, and d) radiation heating up the air when it falls on non-productive space [60]

- There was no consideration of heat exchange with the ground or the structure. It was assumed that all heat gained by the floor and the structure would eventually be transferred to the interior air.
- There was no material exchange with the environment (i.e. infiltration or venting) for the plant factory, it was assumed to be sufficiently sealed.
- Climate regulation is assumed to be consistent throughout a given hour. A potential dynamic or transient approach to temperature regulation (turning equipment on to regulate to a certain minimum (maximum) set point and then waiting until conditions reach the maximum (minimum) set point) may lead to a slight reduction in energy requirements [59]. In general, this study investigates how elements and settings of the climate system can minimise energy consumption, the actual implementation of the climate control is out of the scope of this study (e.g. short burst of fogging instead of continuous operations).
- Wall condensation is assumed to be negligible due to a hydrophobic layer on ETFE and insufficient temperature difference for warmer regions with a polycarbonate cover or in plant factories.
- Condensed water in the dehumidification device is considered to be reused as irrigation or fogging water.
- The nutrient solution was assumed to be at internal air temperature; thus heating or cooling of irrigation water was excluded. Any difference in temperature and thus heat transfer would change the energy balance of the climate control system; however, the same amount of energy would have to be added or removed from the water. It was thus assumed to be negligible.
- The condensation of water vapour for saturated air which experiences a decrease in temperature (in the air to air HEX and refrigeration cycle) was assumed to be instantaneous. The kinetics of this process were excluded.
- Higher solar radiation than the plants require (in summer months or in sunnier regions) was mitigated by whitewash to reduce cooling requirements. Flexible shading screens as an option were not incorporated in the model since the optimisation was done on an hourly basis, which if they had been included would potentially lead to a lower DLI than required. This would cause issues with the comparison of the growing techniques but might be a more energy-efficient way of balancing light with cooling requirements [54].

Plants

- Plants are sufficiently watered and do not experience water or osmotic stress
- Optimum conditions and plant responses to sub-optimal conditions were assumed to be fixed for a specific crop. Any variations caused by different cultivars were out of the scope of this study, the inclusion of a range of crops with different growth and climate characteristics still provide an indication of the effect on energy consumption.
- The increase in plant growth corresponding to a certain increase in daily light integral was fixed as described in 4.2. This response would in reality be slightly different for each crop and depends on how close to saturation the light level already is.
- It was assumed that heat transfer only occurs between the leaves and the air. The growing medium and roots were assumed to be at the same temperature as the surrounding air and thus indirectly included in the energy balance for evapotranspiration.
- The share of absorbed light energy by the plants used for photosynthesis is with <5% low [8] and was hence neglected in the energy balance.
- Variations in leaf area index are not considered as it was assumed that all growth stages of plants are present in a facility to ensure continuous supply [33]
- The mass of water and CO_2 incorporated in the plant biomass is excluded from the comparison as it would be the same for the three systems, can be derived from the plant composition (http://www.fao.org/forestry/17111/en/#:~:text=The%20carbon%20content%20of%20vegetation,by%20oven%2Ddry%20mass).

Other:

- The temperature and solar radiation curves reflect a typical day at the middle of a selected month. The average values to derive the typical days already include fluctuating weather such as cloud cover and rainy days. They are therefore an approximation which facilitate the simulation; since they are averages, the validity of the results is

given but greenhouse climate control may be more challening on days in which the weather deviates substantially from average values.

- The wind speed has indirect influence on infiltration rate and the maximum possible ventilation rate without mechanical support. In this work, it was assumed to be constant (2 m/s). The infiltration rate depends on wind speed and exposure of the greenhouse and was assumed to be constant. This is naturally not always the case but has little effect on the results as infiltration rates are already reported as averages and fluctuations would be flattened out in annual considerations. Similarly, the fan electricity required for ventilation in the OGH might sometimes be higher or lower but the average considered over the year likely results in sufficient accuracy.
- The optimisation did not consider the price changes of electricity throughout the day. It might be that electricity sourced in the morning and late afternoon is most expensive, likely changing the setting for the LEDs slightly if optimised for cost. Further, it could be considered that large CEA facilities produce their own electricity through nearby PV solar fields or wind farms. Short-term storage would then be required, or PV panels could be vertical and double-sided to reflect the increased electricity requirements in the morning and afternoon (https://www.next2sun.de/en/homepage/).
- Further excluded are detailed calculations of the short- and longwave radiation. The considerations for radiative heat gain and reflection are nevertheless incorporated in the equations used by Graamans et al. [30].
- The potential to exchange heat with a host building, if the facility is located on top or below an office or residential building, was not considered in this work. Excess heat from the dehumidification system could be locally utilised as low-grade heat in space heating or warm water preparation.

9 Additional results

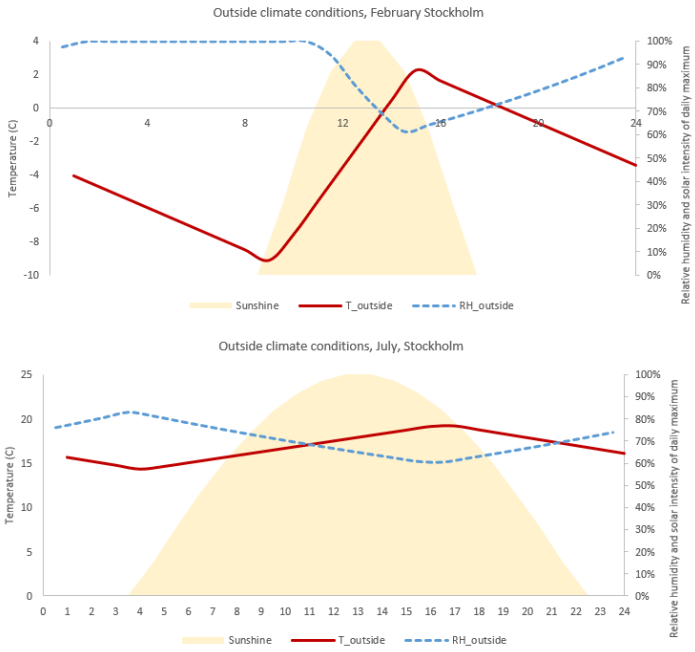

Figure S9: Hourly profile of outside climate conditions in Stockholm during a typical day in February (top) and July (bottom)

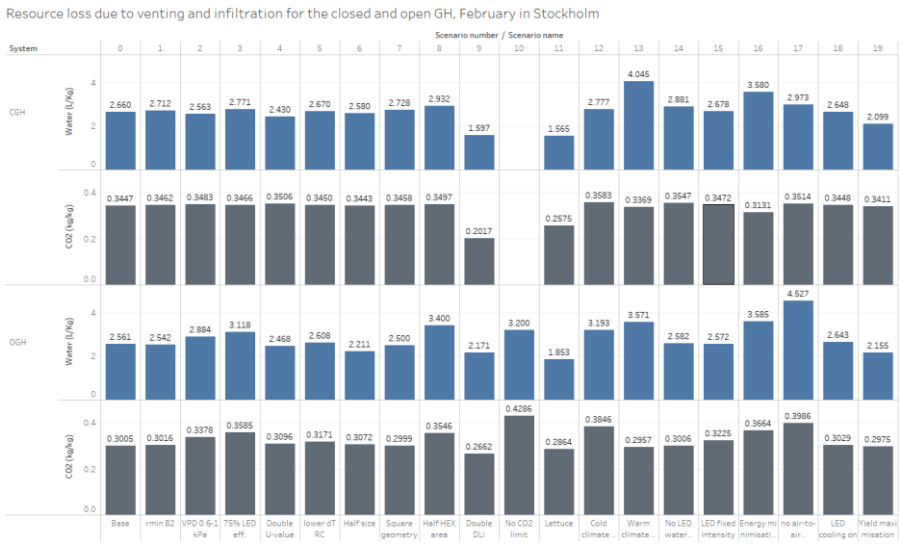

Figure S10: Water and CO_2 loss for the three CEA systems and 18 scenarios for February in Stockholm

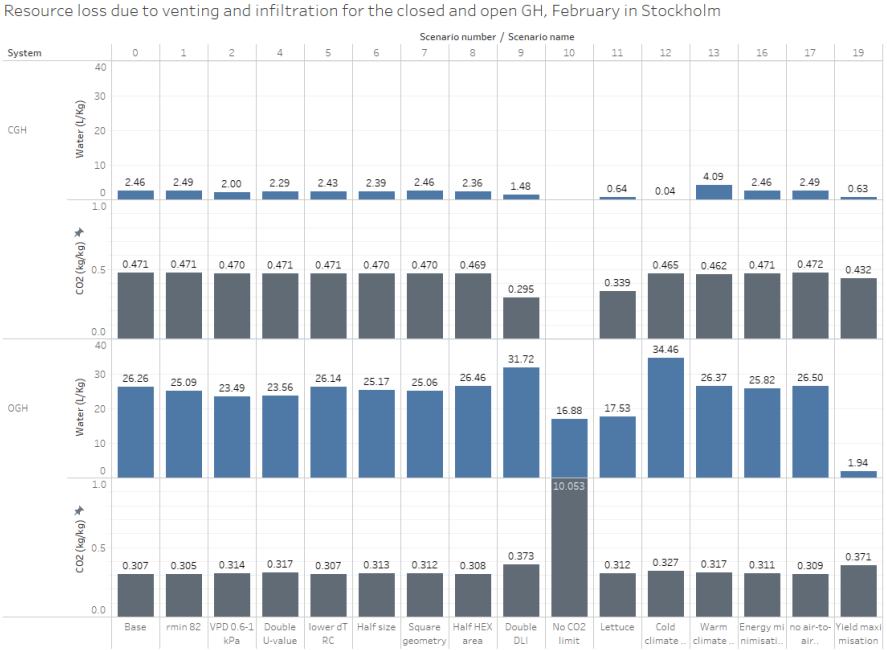

Figure S11: Water and CO_2 loss for the three CEA systems and 18 scenarios for July in Stockholm

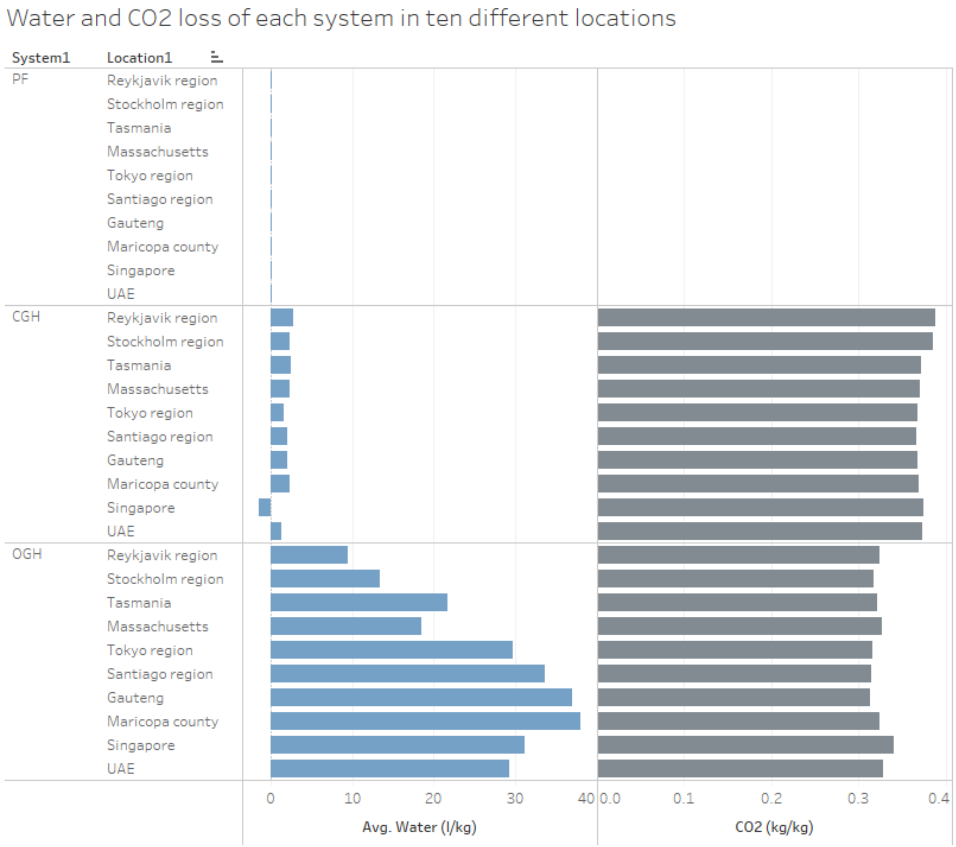

Figure S12:Water and resource loss for the three systems (PF, CGH, OGH) at different locations. Plant uptake of water and CO_2 was not considered in this comparison.

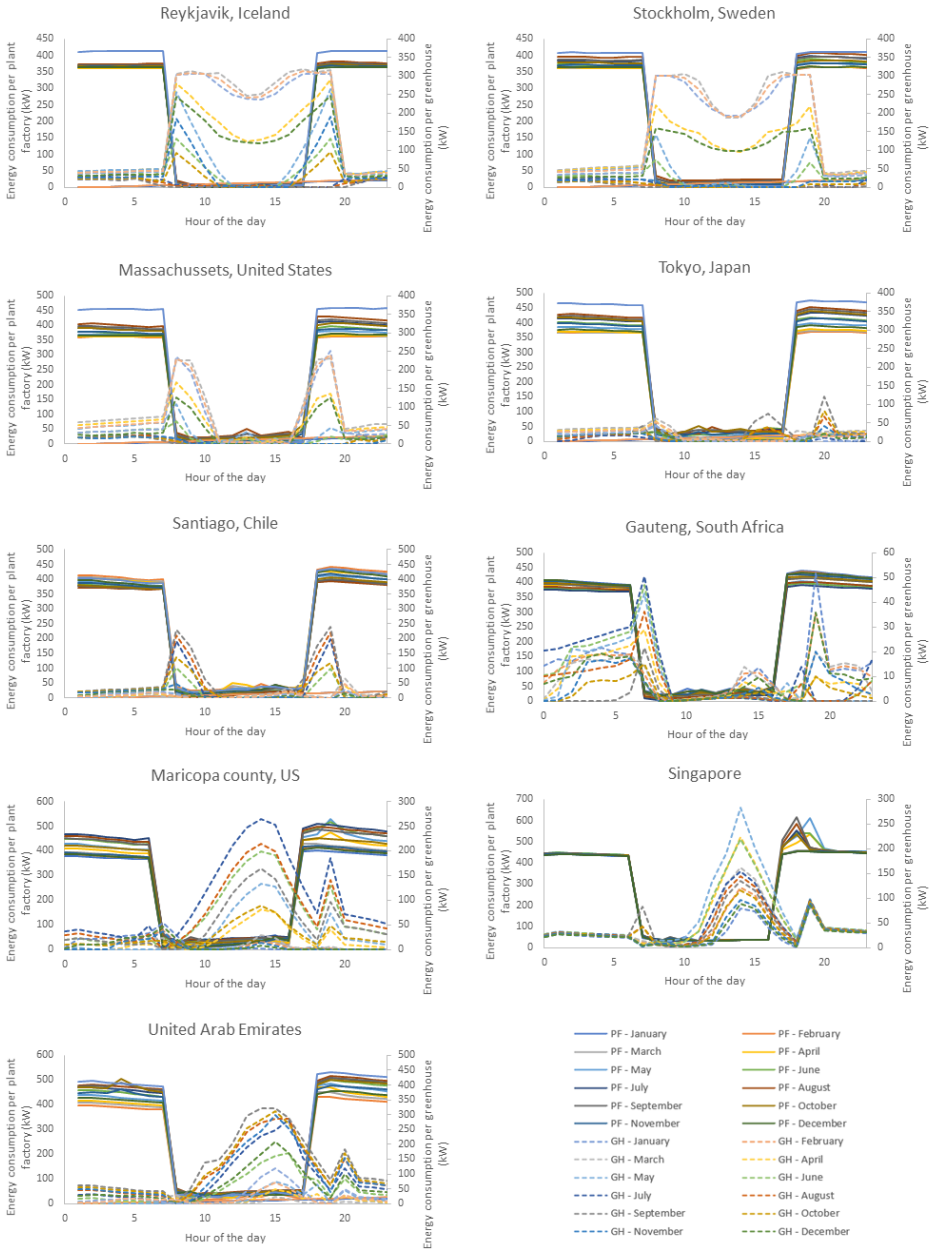

Figure S13: Monthly facility load curves for all regions.The units on the two y-axis are different, the primary (left) y-axis describes the energy consumption of plant factories, the secondary y-axis (right) describes the energy consumption of greenhouses.

Less sunny regions (Reykjavik, Stockholm, Massachusetts, Santiago) rely on supplemental lighting in winter and have thus a high load in the morning and evening hours. Very hot regions required substantial mechanical cooling in the summer months when ventilation was insufficient for climate control. The spikes for plant factories in the afternoon hours are due to less efficient cooling (air-to-air cooling was not feasible anymore) when the daytime temperature was at its highest. The early morning and early evening spikes for greenhouses (especially pronounced in Tokyo and Johannesburg) are due to a change in permissible temperature and humidity ranges between day- and night-time periods. It is important to note that those spikes are only moderate, as indicated by the different scaling of the y-axis on each graph (lowest for Tokyo and Gauteng).

10 Further comparison with other studies

The simulation and optimisation of indoor climate control has been carried out by other studies as well. Similar results were obtained in this for ventilation rates [6], the difference between inside and outside winter temperatures [61], between day and night setpoints [33], and the curves or development of temperature, VPD and evapotranspiration flux during the day [13]. Different results for inside vs outside summer temperatures were obtained by Van Beveren et al. [12], which stems from the influence of temperature on yield considered in this study, as the objective of other control studies was to minimising energy consumption by keeping the temperature within a wide temperature range, rather than optimising for specific energy. Further, relative humidity and temperature during a summer day were different in Katsoulas et al. [17], with lower relative humidity at high temperatures. Although this makes climate control easier, these settings would have violated the maximum VPD of 1.2 in this work. A growers guideline by a leading software provider for vertical farms assumes around 90 W for LEDs and 51.2 W combined for climate control, resulting in 22.1 kWh/kg for the yield and photoperiod assumed in this study [62]. The small discrepancy can partly be explained by the gains through yield-energy optimisation in the present work.

The values from Li et al. [34] used to derive the cooling and specific energy consumption mentioned in the main text in 3.4 included the cooling energy requirements (~1040 kW for the GEG or greenhouse case, ~60 kW for the BC or plant factory case, their figure S1), lighting energy requirements (~40 kW for GEG, ~500 kW for BC), the area (484 m2), photoperiod (11 hours), total annual production (76 tons in the BC and 80.4 tons in the GEG) and supplied DLI levels (24.5 and 34 mol/(m^2*day)for Cai Xin and Xian Cai with the latter constituting 67% of the produce). No information about a COP value could be derived from the documents.

The values for lighting reported in Benis et al. [57] were 47 W/m^2 electricity consumption for 13 hours to achieve 20 mol/(m^2*day). This would equate to a molar efficacy of 9.1 µmol/J which is far above the current range of 2.1 – 3.5 µmol/J for LEDs as described in section S1.7. For the comparison, their reported specific energy consumption in Figure 5 the yield indicated in their Figure 3 was used. The locations had comparable climates the ones used in this study; Lisbon as Gauteng, Paris as Tasmania and New York as Boston. The shipping container was compared with plant factories in this work and rooftop greenhouses with OGHs.

The values used for the comparison with Graamans et al. [7] included the ratio of wet to dry weight (0.07), the dry-weight based specific energy consumption for the GH (115 kWh/kg for UAE, 180 kWh/kg for SWE+ and 70 kWh/kg for NLD), the target DLI of PFs (28.8 mol/(m^2*day)) and obtained yield (71.4 kg/m^2). The share of space conditioning was calculated from the share of cooling compared with the total (e.g. for the PF in UAE, 40 kWh/kg vs. 255 kWh/kg). For the comparison, the cold location in their study (SWE+) was similar to Reykjavik in this work, their temperate location (NLD) was similar to the average between Tasmania and Stockholm in this work.

The values used for the comparison with Harbick and Albright [63] were the energy consumption shown in their Figure 1. The energy for heating (natural gas) was converted to electricity using Equation S171 of this work (which relates target air temperature and outside temperature to the COP of heating), assuming 28 °C as target air temperature and using an average daytime temperature found on www.wikipedia.org. To convert total energy values to weight based values, the area of 1712 m2 was used and as no yield was reported, we assumed equal output. Their DLI was 17 mol/(m^2*day).

The specific energy values derived from the three studies above were adjusted for comparability. This was done by first assuming a 74% proportionality between an increase in DLI and the resulting increase in yield (see Equation S182 in sub-section 4.2 of the SI). Second, a yield adjustment factor was then applied comparing the yields achieved by

adjusting the DLI to the ones reported in this work. For example, Graamans et al. [7] assumed a DLI of 28.8 mol/(m^2*day) to achieve a lettuce yield of 71.4 kg/m^2. This work employed a DLI of 13.7 for the vegetable basket, hence the yield increase factor due to the difference in DLI is 1.81. Multiplying the 40.8 kg/m^2 obtained in this work for plant factory production with 1.81 results in a comparable yield of 74.1 kg/m^2. Hence, their specific energy values were multiplied by 0.96 (71.4 divided by 74.1) .

Nomenclature

Variables

Symbol	Description	Value (unit)
$\frac{\Delta h}{\Delta T}$	Change of saturated air enthalpy between for a given temperature range	kJ/(kg*C)
h_1	Enthalpy of superheated refrigerant before the compressor	kJ/kg
h_{1s}	Enthalpy of saturated refrigerant vapour in the evaporator	kJ/kg
h_2	Enthalpy of the refrigerant after the compressor (assuming non-isentropic expansion)	kJ/kg
h_{2s}	Enthalpy of the refrigerant after the compressor (assuming isentropic expansion)	kJ/kg
h_3	Enthalpy of subcooled refrigerant before the expansion valve	kJ/kg
h_{3s}	Enthalpy of saturated refrigerant liquid in the condenser	kJ/kg
h_4	Enthalpy of refrigerant before the evaporator	kJ/kg
$h_{air,suffix}$	Enthalpy of moist air, dry mass basis	kJ/kg
$h_{sat,cond}$	Enthalpy of the saturated refrigerant vapour in the condenser	kJ/kg
$h_{w,T_{equiv}}$	Enthalpy of condensed water	kJ/kg
A_{suffix}	Respective area of the roof (roof), cardinal direction facing walls (walls,E/S/W/N), all walls (façade), sum of all plant beds (growing), intersectional area or width * times (sect)	m^2
$C_{CO2,centre}$	CO_2 concentration in the air in the centre of the facility	Mol CO_2/mol of air
$C_{CO2,target}$	Target CO_2 concentration in the air	Mol CO_2/mol of air
$C_{air,ext}$	Heat capacity rate external air	J/K
$C_{air,int,1}$	Heat capacity rate internal air for cooling only (decrease in temperature, no condensation)	J/K
$C_{air,int,23}$	Heat capacity rate internal air cooling and condensation (decrease in temperature and ω)	J/K
C_{min}	Smaller heat capacity rate of respective air flows (1 for cooling only, 23 for cooling and condensation)	J/K
C_r	Heat capacity rate ratio of respective air flows	-
C_w	Heat capacity of water	4.19 kJ/(kg*C)
E_{heat}	Electricity consumption of the air-source heat pump	W

E_{ASHP}	Electricity consumption of HVAC heating coil (heat pump)	W
E_{RC}	Electricity consumption of HVAC refrigeration system	W
$E_{comp,ref}$	Electricity consumption of the compressor in the refrigeration cycle	W
$E_{cool,LED}$	Electricity consumption of LED cooling system	W
$E_{fan,ref,ext}$	Electricity consumption of the fan in the air-cooled condenser of the refrigeration cycle	W
$E_{fan,ref,int}$	Electricity consumption of the internal air fan to overcome the pressure drop in the finned tube heat exchanger of the refrigeration cycle	W
$E_{fans,hvac}$	Electricity consumption fans in HVAC system	W
$E_{fans,a2a,ext}$	Electricity consumption of the external air fans for the air to air HEX	W
$E_{fans,a2a,int}$	Electricity consumption of the internal air fans for the air to air HEX	W
$E_{fans,vent}$	Electricity consumption venting fans	W
E_{fog}	Electricity consumption of fogging system (OGH only)	W
E_{total}	Total electricity consumption	W
E_{vent}	Electricity consumption of venting fans	W
E_{vent}	Electricity consumption of ventilation system (OGH only)	W
F_{hvac}	Dry mass flow of hvac system	Kg/s
$F_{GH,in}$	Dry air mass flow rate entering the GH	Kg/s
$F_{air,a2a,ext}$	Outside air flow in the plate HEX	Kg/s
$F_{air,a2a,int}$	Internal air flow in the plate HEX	Kg/s
$F_{air,cond,req}$	Required outside air flow in the air-cooled condenser of the refrigeration cycle	Kg/s
F_{vent}	Dry mass flow of ventilation system (OGH only)	Kg/s
F_{vent}	Dry air mass flow rate of venting air	Kg/s
$I_{LED,canopy}$	Radiation of the LEDs received by the plany bed	W_{PAR}/m^2
I_{LED}	Radiation of the LEDs at the light fixture	W_{PAR}/m^2
$I_{net,PAR}$	Net radiation, solar and LED combined (PAR)	W_{PAR}/m^2
I_{net}	Net radiation, solar and LED combined (full spectrum)	W/m^2
$I_{solar,sky}$	Irradiation	$Wh/(m^2*h)$
$I_{solar,eff}$	Irradiation reaching into the greenhouse	$Wh/(m^2*h)$
I_{target}	The intensity of combined solar and LED radiation which approximates a uniform light supply	W_{PAR}/m^2
$PPFD_{LED}$	Photosynthetic photon flux density	$\mu mol/(m^2*s)$
$Power_{LED}$	Power consumption per unit area of LED	W_e/m^2
$P_{sat,suffix}$	Water vapour pressure of saturated air	hPa
$P_{w,suffix}$	Water vapour pressure	hPa
$Q_{1,actual}$	The cooling duty realised for the cooling-only step (1)	W

$Q_{1,est}$	The estimated cooling duty for the cooling-only step (1) used to calculate the error and thus adjustment of $f_{cooling\ ratio}$	W
$Q_{1,max}$	The theoretical maximum cooling duty based on the initial temperature difference (between outside air and hvac inlet air) and the lower heat capacity rate	W
$Q_{1,pot}$	The theoretical cooling duty for the cooling-only step (1) according to the NTU method	W
$Q_{1,req}$	The required cooling duty to bring the temperature of the internal air to $T_{condens}$	W
$Q_{23,actual}$	The cooling duty realised for the cooling and condensation step (23)	W
$Q_{23,check}$	The maximum cooling duty that can be realised based on the HEX area share and the temperature driving force	W
$Q_{23,final}$	The cooling duty obtained for step 23 after the successive iterations	W
$Q_{23,max}$	The theoretical maximum cooling duty based on the initial temperature difference (between the outside air and $T_{condens}$) and the lower heat capacity rate	W
$Q_{23,pot}$	The theoretical cooling duty for the cooling and condensation step (23) according to the NTU method	W
$Q_{23,req}$	The required cooling duty to bring the temperature of the internal air from $T_{condens}$ to $T_{air,hvac,out}$	W
$Q_{heat,ASHP}$	Remaining heating duty to be realised by the air-source heat pump	W
$Q_{LED,heat}$	Heat gain from the waste heat of the LEDs	W
$Q_{LED,PAR}$	Heat gain from the light of the LEDs not absorbed by plants	W
Q_{PF}	Heat transfer between the plant factory and the environment	W
$Q_{R134A,cool}$	Cooling requirements of the hot refrigerant	W
$Q_{R134A,remain}$	Remaining cooling duty of the hot refrigerant	W
$Q_{cool,LED}$	Water cooling of LED cooling load	W
$Q_{cool,remain,a2a}$	The remaining cooling load to be realised by the refrigeration cycle	W
$Q_{fans,hvac}$	Heat gain from fans in hvac system	W
Q_{fog}	Sensible heat removed through fogging	W
$Q_{infiltration}$	Energy gain or loss due to infiltrating air	W
$Q_{max,1,check}$	The theoretical maximum cooling duty based on the initial temperature difference (between the outside air after step 23 and the internal air at the hvac inlet) and the lower heat capacity rate	W
$Q_{recovery,actual}$	Heat recovery duty realised by the hot refrigerant	W
$Q_{recovery,pot}$	Potential heat recovery between the internal air and the hot refrigerant	W
$Q_{ref,pot}$	Theoretical maximum cooling load dependent on the temperature driving force	W
Q_{solar}	Heat gain from solar radiation not absorbed by plants	W

$Q_{structure}$	Heat transfer between the building structure and the environment	W
Q_{total}	Total heat balance	kW
R_a	Individual gas constant air	J/(kg*K)
R_w	Individual gas constant water vapour	J/(kg*K)
T_1	Superheated refrigerant temperature before the compressor	C
T_{1s}	Evaporator temperature in the refrigeration cycle	C
T_3	Subcooled refrigerant temperature before the expansion valve	C
T_{3s}	Condenser temperature in the refrigeration cycle	C
$T_{air,equiv}$	Target temperature for required condensation (Ps@T_equiv = Pw,hvac,out)	C
$T_{air,ext,post-cond}$	The temperature of the outside air after the cooling and condensation step (23)	C
$T_{air,int,a2a,out}$	The internal air temperature after the air to air HEX	C
$T_{air,int,post-cond}$	The temperature of the internal air exiting the air to air HEX	C
$T_{air,suffix}$	Air temperature at given location	C
$T_{condens}$	Saturation temperature of the internal air at its water vapour pressure at the inlet of the hvac	C
T_{leaf}	Temperature of leaf surface	C
T_{max}	Maximum growing temperature of specific crop	C
T_{opt}	Optimum growing temperature of specific crop	C
$T_{outside,out,max}$	Maximum outlet temperature of the outside air in the air-cooled condenser of the refrigeration cycle	C
U_{hex}	Heat transfer coefficient for heat exchanger, either air to air (a2a) or refrigeration cycle finned tube (ref)	W/(m2*C)
U_{GH}	Overall heat transfer coefficient for the greenhouse structure	W/(m2*C)
U_{GH}	Overall heat transfer coefficient for the greenhouse structure	W/(m2*C)
$V_{hvac,out}$	Volumetric flowrate at exit of HVAC system	m^3/s
Vol	Volume of CEA facility	m^3
X_{suffix}	Absolute humidity	g/m^3
Y_{hourly}	Attributed hourly yield	$Kg/(m^2*h)$
$Y_{ref,annual}$	Annual reported yield for year-round growing for specific crop at reference conditions	$Kg/(m^2*year)$
f_D	Darcy friction factor	-
$f_{LED\ cooling}$	Share of LED waste heat water cooled, 1 in PF	%
$f_{a2a,share}$	Share of total hvac flow sent through plate HEX (optimisation variable)	%
$f_{cooling\ ratio}$	Ratio of the area considered to be used for the cooling-only (1) step versus the total HEX area	%
$m_{CO2,loss}$	Mass of CO_2 lost	Kg/s

$m_{R134A,ref}$	Refrigerant flowrate	Kg/s
$m_{w,balance}$	Water lost or collected to environmental exchange	g/s
$m_{w,evap}$	Mass of water evaporated from plants	Kg H_2O/s
$m_{w,fog}$	Mass of water flow through fogging device	kg/s
$m_{w,infiltration}$	Mass of water introduced through venting	Kg/s
$m_{w,loss}$	Water lost to the environment due to infiltration and venting during a 24 hour period	g/day
$m_{w,out}$	Flowrate of condensed water	kg/s
n_{CO2}	Moles of CO2 in the growing facility	mol
$n_{air,vent}$	Molar flowrate air venting	Mol/s
r_a	Aerodynamic resistance to transpiration	s/m
r_c	Canopy resistance to transpiration, r_s /2	s/m
s_1	Entropy of the superheated refrigerant before the compressor	kJ/(kg*C)
s_{1s}	Entropy of the saturated refrigerant vapour in the evaporator	kJ/(kg*C)
s_{3s}	Entropy of the saturated refrigerant liquid in the condenser	kJ/(kg*C)
$s_{sat,cond}$	Entropy of the saturated refrigerant vapour in the condenser	kJ/(kg*C)
t_{photo}	Daily photoduration	h/day
$u_{air,a2a,ext}$	Outside air velocity in the plate HEX (optimisation variable)	m/s
$u_{air,a2a,int}$	Internal air velocity in the plate HEX	m/s
$u_{air,cond}$	Velocity of outside air in the air-cooled condenser of the refrigeration cycle	m/s
$u_{air,int,ref}$	Internal air velocity in the finned tube HEX (evaporator) of the refrigeration cycle	m/s
$u_{vent,out}$	Velocity of air through vent openings	m/s
ΔP_{hvac}	Pressure drop in the HVAC duct	Pa
ΔP_{plate}	The pressure drop of internal and external air within the plate HEX	Pa
ΔP_{vent}	Static and dynamic pressure drop delivered by the venting fans	Pa
AER_{hvac}	Air exchange rate of HVAC system	AE/h
AER_{vent}	Air exchange rate of ventilation system (only OGH, 0 for PF and CGH)	AE/h
$CO2_{loss}$	Carbon dioxide lost to the environment due to infiltration and venting	Kg/s
COP_{heat}	Coefficient of Performance for heating of HVAC cooling system	-
COP_{ASHP}	Coefficient of performance of the air-source heat pump	-
COP_{comp}	Coefficient of performance of the compressor in the refrigeration cycle	-
$COP_{cool,LED}$	Coefficient of Performance of LED cooling system	

COP_{cool}	Coefficient of Performance for cooling of HVAC cooling system	-
$DLI_{LED,canopy}$	Total moles of light received by the plant canopy	Mol PAR/(m2*day)
DLI_{LED}	Total moles of light produced by the LEDs	Mol PAR/(m2*day)
$DLI_{natural}$	Daily light integral solar radiation	Mol PAR/(m2*day)
DLI_{plant}	Daily light integral required	Mol PAR/(m2*day)
ET	Evapotranspiration	Kg/(h*m^2) or mm/h
$Error$	The error between the estimated and actual cooling duty for step 1	-
LH	Latent heat transfer from plants to environment due to transpiration	W/m^2
$LMTD_{23,check}$	The log-mean temperature difference for the heat exchange in in the cooling and condensation step	C
$LMTD_{recovery}$	Log mean temperature difference in the condenser of the refrigeration cycle, assuming reheating of internal air	C
$LMTD_{ref}$	Log mean temperature difference in the evaporator of the refrigeration cycle	C
NTU	Number of transfer units	-
Nu	Nusselt number	-
PAR_{LED}	PAR	mol/(m^2*h)
Pr	Prandtl number	-
Re	Renold's number	-
SE_{hourly}	Specific energy consumption (for given hour of photoperiod)	Wh/kg
$SE_{product}$	Specific energy consumption as average during one month (or year)	Wh/kg
SH	Sensible heat transfer from plants to environment due to evapotranspiration balance	W/m^2
VCD	Vapour concentration difference at the leaf surface	g/m^3
VPD_{leaf}	Vapour pressure difference between air and saturated air at the leaf surface temperature	hPa
VPD_{suffix}	Vapour pressure difference of air	hPa
Vol	Volume of greenhouse or plant factory	m^3
YF_{CO2}	Yield factor due to varying CO_2 concentration in the air	-
YF_T	Yield factor due to varying air temperature	-
YF_{total}	Product of all yield factors for a given hour	-
α	Surface heat transfer coefficient	W/(m^2*C)
ϵ	Heat exchanger effectiveness	-
λ_{suffix}	Latent heat of vapourisation at the temperature of the location indicated by the suffix	kJ/kg
$\rho_{air,suffix}$	Density of dry air	Kg/m^3
ρ_{suffix}	Density of wet air	Kg/m^3
ω_{suffix}	specific humidity ~~Mixing ratio~~ of water in air	g/kg

Suffixes

Location	Description
center	Air condition at the center zone (half-way between East and West wall) of the GH or PF
equiv	Air condition after the condensation step in the HVAC system
hvac,in	Air condition at the inlet of the HVAC system
hvac,out	Air condition at the outlet of the HVAC system
In	Air condition at the inlet zone of the facility, influenced by the hvac_out flow and venting (OGH)
leaf	Air and water conditions at the leaf surface of the plants
out	Air condition at the exit zone of the facility, which is also hvac_in and the venting outlet
outside	Air condition at the outside of the facility

Fixed variables

Name	Description	Value (unit)	Source
$\dot{m}_{CO2,supply,ma}$	Maximum CO_2 dosing capacity per unit area	0.015 kg/(m²*hr)	Based on 150 kg/ha/h [64]
$\dot{m}_{w,fog,max}$	Maximum fogging capacity per unit area	0.5 kg/(m²*hr)	[5]
ΔT_{sub}	Extent of refrigerant subcooling	-9 C	[9]
ΔT_{sup}	Extent of refrigerant superheating	5 C	[9]
$A_{hex,a2a}$	Heat transfer area of plate HEX	9,600 m²	Based on design for feasible dimensions and potential to cover cooling load with reasonable COP when outside temperatures are below 0 C
$A_{hex,ref,ext}$	Finned Hex area (condenser) of the refrigeration cycle	6,432 m²	Based on design for feasible dimensions and ability to cool down the refrigerant with outside air for the maximum hvac cooling load (~750 kW)
$A_{hex,ref,int}$	Finned Hex area (evaporator) of the refrigeration cycle	3,618 m²	Based on design for feasible dimensions and ability to cool down the refrigerant with outside air for the maximum hvac cooling load (~750 kW)
A_{duct}	Duct intersectional area of HVAC system	2.32 m²	Designed for 12 m/s, 10 AE/h and 10,000 m3
$A_{face,ref,int}$	Face area of the finned tube HEX (evaporator) of the refrigeration cycle	9 m²	Based on design for feasible dimensions and ability to cool down the refrigerant with outside air for the maximum hvac cooling load (~750 kW)

A_{fch}	Area of each channel between two plates in the plate HEX	0.032 m^2	http://www.heattransferconsult.nl/Tradi_Plate_Calc.html
C_1	First radiation term for rs	90.1	Based on empirical model constructed from experimental measurements from Graamans et al. [7] and Pamungkas et al. [46]
C_2	2nd radiation term for rs	11.3	Based on empirical model constructed from experimental measurements from Graamans et al. [7] and Pamungkas et al. [46]
C_3	VPD term for rs	4.3	Based on empirical model constructed from experimental measurements from Graamans et al. [7] and Pamungkas et al. [46]
C_4	CO_2 term for rs	6.1E-07	[47]
$C_{CO2,amb}$	Ambient CO_2 concentration in the air	415 ppm	
$C_{CO2,ref}$	Reference CO_2 concentration in the air for yield figures	800 ppm	[52]
$C_{p,air}$	Heat capacity of air	1.005 kJ/(kg*K)	
$C_{p,liquid}$	Refrigerant liquid heat capacity	1.44 kJ/(kg*K)	https://www.gas-servei.com/images/Technical-data-sheet-R134a-ENGLISH.pdf
$C_{p,vapour}$	Refrigerant vapour heat capacity	0.85 kJ/(kg*K)	https://www.gas-servei.com/images/Technical-data-sheet-R134a-ENGLISH.pdf
C_w	Heat capacity of liquid water	4.19 kJ/(kg*K)	
$D_{hex,equiv}$	Equivalent diameter for air flow across the finned tubes	0.0254 m	Outer tube diameter used as pitch between tube
D_{hyd}	Hydraulic diameter	0.016 m	http://www.heattransferconsult.nl/Tradi_Plate_Calc.html

	for the plates in the plate HEX		
D_{duct}	Duct diameter of HVAC system	1.72 m	Designed for 12 m/s, 10 AE/h and 10,000 m^3
D_{leaves}	Average leaf diameter	0.08 m	[29,30]
D_{plate}	Distance between plates in plate HEX	0.008 m	Based on design for feasible dimensions and potential to cover cooling load with reasonable COP when outside temperatures are below 0 C
$E_{fog,ref}$	Reference electricity consumption of fogging system	2.41 Wh/l	Calculated assuming 70 bar pressure (http://www.fogsis.com/haber-fogging-system-and-efficient-greenhouse-79.html) using pump head (https://www.engineeringtoolbox.com/pump-head-pressure-d_663.html) and power consumption relations (https://www.engineeringtoolbox.com/water-pumping-costs-d_1527.html)
L_{plate}	Length of the plate in the plate HEX	12 m	Based on design for feasible dimensions and potential to cover cooling load with reasonable COP when outside temperatures are below 0 C
N_{plate}	Number of plates in plate HEX	200	Based on design for feasible dimensions and potential to cover cooling load with reasonable COP when outside temperatures are below 0 C
N_{racks}	Number of growing racks	4 (PF), 1 (GH)	Assumption for PF based on building height 8m and stack height 1.5m
$\frac{PAR_{canopy}}{PAR_{LED}}$	Share of LED light reaching the plant bed	89% for plant factories (due to reflective surfaces within the racks), 79% for greenhouses	[31]
$P_{air,atm}$	Ambient pressure	101325 Pa	
$T_{evap,LED}$	Temperature in the evaporator (refrigerant) for LED cooling	10 C	15 C as difference assumed, LEDs kept at 25 C

U_{cover}	Overall heat transfer coefficient for the cover	2 ETFE, 2.27 PC, 0.5 RLC W/(m^2*C)	[2,4]
U_{wall}	Overall heat transfer coefficient for the wall or building	0.3 W/(m^2*C)	[65]
W_{plate}	Width of plate in plate HEX	4 m	Based on design for feasible dimensions and potential to cover cooling load with reasonable COP when outside temperatures are below 0 C
a_{air}	Thermal diffusivity air	1E-07*T+2E-05 m^2/s	https://www.me.psu.edu/cimbala/me433/Links/Table_A_9_CC_Properties_of_Air.pdf
$f_{LED,cooling}$	Share of waste heat absorbed by water cooling	0 – 0.85	Decision variable in optimisation, maximum of 85% from Mechatronix (Personal communication)
$f_{production}$	Share of the ground area used for plant beds	82% (GH), 60% (PF)	GH: (Villarreal-Guerrero et al., [13], PF: assumption based on higher requirements for machinery, automation and higher growing racks
$f_{radiation}$	Factor accounting for radiative heat loss	20%	[65]
$f_{shading}$	Effect on solar transmissivity through structural shading	95 %	Assumption based on typical greenhouse design
$f_{screen,EW}$	Thermal day screen covering East (afternoon) and West (morning) facing walls	100% (off), 57% (on)	https://fyi.extension.wisc.edu/energy/files/2016/09/ThermalCurtains.pdf
f_{screen}	Thermal night screen covering	100% (off), 57% (on)	https://fyi.extension.wisc.edu/energy/files/2016/09/ThermalCurtains.pdf

$f_{vent\ size}$	Typical share of vent opening compared with GH height	19%	[10]
$f_{whitewash}$	Whitewash for reduced solar light transmission	75% for light and 50% for strong	[11]
k_s	Reflection coefficient	0.7	[29]
$r_{s,min}$	Minimum stomatal resistance to transpiration	29 s/m	Based on empirical model constructed from experimental measurements from Graamans et al. [7] and Pamungkas et al. [46]
$\Delta T_{cond,outside}$	Temperature difference between air and refrigerant in the condenser	15 C	[9]
$\Delta T_{cond,outside}$	Minimum temperature difference between the evaporator and condenser operating temperature and the evaporator and inlet air stream	5 C	Assumption based on conversation with HVAC professional
ΔT_{evap}	Temperature difference between air and refrigerant in the evaporator	8 C	[9]

$\Delta T_{min,R134a,air}$	Minimum approach temperature between outside air and refrigerant in the condenser	3 C	Chosen to ensure sufficient heat transfer with given design of the air-cooled condenser in the refrigeration cycle
$AER_{hvac,max}$	Maximum air exchange rate in the HVAC system	100 AE/h	Assumption
$AER_{infiltration}$	Equivalent air exchange rate from air infiltration	0.25 AE/h	[66]
$AER_{vent,max}$	Maximum ventilation rate	40 AE/h	Assumption
AER_{min}	Minimum air exchange rate in the factility	0.75 AE/h	Assumption to ensure sufficient air flow to distribute CO_2, moisture and heat
CAC	Cumulative area cover, share of plant leaf cover in plant bed	90%	[7]
LAI	Leaf area index	2.1 (lettuce), 2.8 (tomato)	[30,54]
MW_{h2o}	Molecular weight water	18 g/mol	
MW_{CO2}	Molecular weight CO_2	44.01 g/mol	
MW_{air}	Molecular weight air	28.96 g/mol	
R	Specific gas constant	8.314 J/(mol*K)	
Ra	Individual gas constant air	286.9 J/(kg*K)	

Rw	Individual gas constant water vapour	461.5 J/(kg*K)	
VPD_{max}	Maximum permissible vapour pressure deficit	12 hPa	[67]
VPD_{min}	Minimum permissible vapour pressure deficit	4 hPa	[67]
YF_{rad}	Yield factor influenced by the radiation	1 for default (reference), 1.74 for "high lighting"	[7,52]
dh/ds	Entropy dependency on temperature for refrigerant vapour	325 1/C	https://www.ohio.edu/mechanical/thermo/property_tables/r134a/ph_r134a.html
ξ	Minor Dynamic Loss Coefficient	4.15	4*0.7 (90° bend with vanes) + 1 (flow from duct) + 0.35 (flow away from duct) https://www.engineeringtoolbox.com/minor-loss-air-ducts-fittings-d_208.html
η_{LED}	Conversion efficiency LED	0.52 W_{PAR} / W_e	[7]
η_{fans}	Fan efficiency	65%	[9]
η_{fog}	Fogging system efficiency (share of water droplets evaporated before falling to the ground)	68%	[6]
λ_{air}	Thermal conductivity air	8E-05*T+0.0241 W/(m*C)	https://www.me.psu.edu/cimbala/me433/Links/Table_A_9_CC_Properties_of_Air.pdf

λ_{tube}	Thermal conductivity of tube or plate (copper core with aluminium fins)	380 W/(m*C)	[9]
μ_{air}	Dynamic viscosity air	5E-08*T+2E-05 Pa s	https://www.me.psu.edu/cimbala/me433/Links/Table_A_9_CC_Properties_of_Air.pdf
ν_{air}	Kinematic viscosity air	9E-08*T + 1E-05 m^2/s	https://www.me.psu.edu/cimbala/me433/Links/Table_A_9_CC_Properties_of_Air.pdf
τ_{cover}	Solar transmissivity	83% (ETFE), 70% (PC), 28% (RLC)	[2]
$\epsilon_{surface}$	Surface roughness	0.0000015 m	https://www.pumpfundamentals.com/PIPE%20ROUGHNESS%20VALUES.pdf

References

[1] Choab N, Allouhi A, El Maakoul A, Kousksou T, Saadeddine S, Jamil A. Review on greenhouse microclimate and application: Design parameters, thermal modeling and simulation, climate controlling technologies. Sol Energy 2019;191:109–37. https://doi.org/10.1016/j.solener.2019.08.042.

[2] Proksch G. Creating Urban Agricultural Systems - An Integrated Approach to Design. New York: Routledge; 2017.

[3] Rasheed A, Lee JW, Lee HW. Development and optimization of a building energy simulation model to study the effect of greenhouse design parameters. Energies 2018;11. https://doi.org/10.3390/en11082001.

[4] Pakari A, Ghani S. Evaluation of a novel greenhouse design for reduced cooling loads during the hot season in subtropical regions. Sol Energy 2019;181:234–42. https://doi.org/10.1016/j.solener.2019.02.006.

[5] Vanthoor BHE, Gázquez JC, Magán JJ, Ruijs MNA, Baeza E, Stanghellini C, et al. A methodology for model-based greenhouse design: Part 4, economic evaluation of different greenhouse designs: A Spanish case. Biosyst Eng 2012;111:336–49. https://doi.org/10.1016/j.biosystemseng.2011.12.008.

[6] Villarreal-Guerrero F, Kacira M, Fitz-Rodríguez E, Linker R, Kubota C, Giacomelli GA, et al. Simulated performance of a greenhouse cooling control strategy with natural ventilation and fog cooling. Biosyst Eng 2012;111:217–28. https://doi.org/10.1016/j.biosystemseng.2011.11.015.

[7] Graamans L, Baeza E, van den Dobbelsteen A, Tsafaras I, Stanghellini C. Plant factories versus greenhouses: Comparison of resource use efficiency. Agric Syst 2018;160:31–43. https://doi.org/10.1016/j.agsy.2017.11.003.

[8] Kozai T, Niu G, Takagaki M. Plant Factory - An Indoor Vertical Farming System for Efficient Quality Food Production. Academic Press; 2019.

[9] Graamans L, Tenpierik M, van den Dobbelsteen A, Stanghellini C. Plant factories: Reducing energy demand at high internal heat loads through façade design. Appl Energy 2020;262:114544. https://doi.org/10.1016/j.apenergy.2020.114544.

[10] Vanthoor BHE, Stanghellini C, Van Henten EJ, De Visser PHB. A methodology for model-based greenhouse design: Part 1, a greenhouse climate model for a broad range of designs and climates. Biosyst Eng 2011;110:363–77. https://doi.org/10.1016/j.biosystemseng.2011.06.001.

[11] Vanthoor BHE, Stigter JD, van Henten EJ, Stanghellini C, de Visser PHB, Hemming S. A methodology for model-based greenhouse design: Part 5, greenhouse design optimisation for southern-Spanish and Dutch conditions. Biosyst Eng 2012;111:350–68. https://doi.org/10.1016/j.biosystemseng.2012.01.005.

[12] Van Beveren PJM, Bontsema J, Van Straten G, Van Henten EJ. Minimal heating and cooling in a modern rose greenhouse. Appl Energy 2015;137:97–109. https://doi.org/10.1016/j.apenergy.2014.09.083.

[13] Villarreal-Guerrero F, Kacira M, Fitz-Rodríguez E, Kubota C, Giacomelli GA, Linker R, et al. Comparison of three evapotranspiration models for a greenhouse cooling strategy with natural ventilation and variable high pressure fogging. Sci Hortic (Amsterdam) 2012;134:210–21. https://doi.org/10.1016/j.scienta.2011.10.016.

[14] Ghoulem M, El Moueddeb K, Nehdi E, Boukhanouf R, Kaiser Calautit J. Greenhouse design and cooling technologies for sustainable food cultivation in hot climates: Review of current practice and future status. Biosyst Eng 2019;183:121–50. https://doi.org/10.1016/j.biosystemseng.2019.04.016.

[15] Kittas C, Boulard T, Papadakis G. Natural ventilation of a greenhouse with ridge and side openings: Sensitivity to temperature and wind effects. Trans Am Soc Agric Eng 1997;40:415–25. https://doi.org/10.13031/2013.21268.

[16] Zhi Z, Gates RS, Zhirong Z, Xiaohui H. Evaluation of ventilation performance and energy efficiency of greenhouse fans. Int J Agric Biol Eng 2015;8:103–10. https://doi.org/10.3965/j.ijabe.20150801.014.

[17] Katsoulas N, Sapounas A, De Zwart F, Dieleman JA, Stanghellini C. Reducing ventilation requirements in semi-closed greenhouses increases water use efficiency. Agric Water Manag 2015;156:90–9. https://doi.org/10.1016/j.agwat.2015.04.003.

[18] Van Henten EJ. Validation of a dynamic lettuce growth model for greenhouse climate control. Agric Syst

1994;45:55–72. https://doi.org/10.1016/S0308-521X(94)90280-1.

[19] Tewolde FT, Shiina K, Maruo T, Takagaki M, Kozai T, Yamori W. Supplemental LED inter-lighting compensates for a shortage of light for plant growth and yield under the lack of sunshine. PLoS One 2018;13:1–14. https://doi.org/10.1371/journal.pone.0206592.

[20] Weidner T, Yang A. The potential of urban agriculture in combination with organic waste valorization: Assessment of resource flows and emissions for two european cities. J Clean Prod 2019;244:118490. https://doi.org/10.1016/j.jclepro.2019.118490.

[21] Reyes-Rosas A, Molina-Aiz FD, Valera DL, López A, Khamkure S. Development of a single energy balance model for prediction of temperatures inside a naturally ventilated greenhouse with polypropylene soil mulch. Comput Electron Agric 2017;142:9–28. https://doi.org/10.1016/j.compag.2017.08.020.

[22] Stacey NT, Hildebrandt D. Quantitative modeling of a greenhouse as a bioreactor to process power station emissions. Environ Prog Sustain Energy 2018;37:1774–80. https://doi.org/10.1002/ep.12824.

[23] Zhang S, Schulman B. A Numerical Model for Simulating the Indoor Climate inside the Growing Chambers of Vertical Farms with Case Studies. Int J Environ Sci Dev 2017;8:728–35. https://doi.org/10.18178/ijesd.2017.8.10.1047.

[24] He X, Wang J, Guo S, Zhang J, Wei B, Sun J, et al. Ventilation optimization of solar greenhouse with removable back walls based on CFD. Comput Electron Agric 2018;149:16–25. https://doi.org/10.1016/j.compag.2017.10.001.

[25] López A, Valera DL, Molina-Aiz FD, Peña A. Sonic anemometry to evaluate airflow characteristics and temperature distribution in empty Mediterranean greenhouses equipped with pad-fan and fog systems. Biosyst Eng 2012;113:334–50. https://doi.org/10.1016/j.biosystemseng.2012.09.006.

[26] Teitel M, Ziskind G, Liran O, Dubovsky V, Letan R. Effect of wind direction on greenhouse ventilation rate, airflow patterns and temperature distributions. Biosyst Eng 2008;101:351–69. https://doi.org/10.1016/j.biosystemseng.2008.09.004.

[27] Arbel A, Yekutieli O, Barak M. Performance of a fog system for cooling greenhouses. J Agric Eng Res 1999;72:129–36. https://doi.org/10.1006/jaer.1998.0351.

[28] Wang XW, Luo JY, Li XP. CFD based study of heterogeneous microclimate in a typical chinese greenhouse in central China. J Integr Agric 2013;12:914–23. https://doi.org/10.1016/S2095-3119(13)60309-3.

[29] Katsoulas N, Stanghellini C. Modelling crop transpiration in greenhouses: Different models for different applications. Agronomy 2019;9:1–17. https://doi.org/10.3390/agronomy9070392.

[30] Graamans L, van den Dobbelsteen A, Meinen E, Stanghellini C. Plant factories; crop transpiration and energy balance. Agric Syst 2017;153:138–47. https://doi.org/10.1016/j.agsy.2017.01.003.

[31] Kozai T. Resource use efficiency of closed plant production system with artificial light: Concept, estimation and application to plant factory. Proc Japan Acad Ser B Phys Biol Sci 2013;89:447–61. https://doi.org/10.2183/pjab.89.447.

[32] Hemming S, De Zwart F, Elings A, Righini I, Petropoulou A. Remote control of greenhouse vegetable production with artificial intelligence—greenhouse climate, irrigation, and crop production. Sensors (Switzerland) 2019;19. https://doi.org/10.3390/s19081807.

[33] Golzar F, Heeren N, Hellweg S, Roshandel R. A novel integrated framework to evaluate greenhouse energy demand and crop yield production. Renew Sustain Energy Rev 2018;96:487–501. https://doi.org/10.1016/j.rser.2018.06.046.

[34] Li L, Li X, Chong C, Wang CH, Wang X. A decision support framework for the design and operation of sustainable urban farming systems. J Clean Prod 2020;268:121928. https://doi.org/10.1016/j.jclepro.2020.121928.

[35] Incropera FP, DeWitt DP, Bergman TL, Lavine AS. Fundamentals of Heat and Mass Transfer. 6th ed. John Wiley & Sons; 2006.

[36] Tong Y, Kozai T, Ohyama K. Performance of household heat pumps for nighttime cooling of a tomato greenhouse during the summer. Appl Eng Agric 2013;29:414–21. https://doi.org/10.13031/aea.29.9984.

[37] Ahmadi MH, Ahmadi MA, Sadaghiani MS, Ghazvini M, Shahriar S, Alhuyi Nazari M. Ground source heat pump carbon emissions and ground-source heat pump systems for heating and cooling of buildings: A review. Environ Prog Sustain Energy 2018;37:1241–65. https://doi.org/10.1002/ep.12802.

[38] Sarbu I, Sebarchievici C. General review of ground-source heat pump systems for heating and cooling of buildings. Energy Build 2014;70:441–54. https://doi.org/10.1016/j.enbuild.2013.11.068.

[39] Swamee PK, Jain AK. Explicit equations for pipeflow problems. J Hydraul Div 1976;102.

[40] Branan CA. Rules of Thumb for Chemical Engineers. Gulf Publishing; 1998.

[41] Chopey NP. Handbook of chemical engineering calculations. McGraw-Hill; 2004.

[42] GPSA. Engineering Data Book. 12th FPS. Gas Processors Suppliers Association; n.d.

[43] Serth RW, Lestina T. Process heat transfer: Principles, applications and rules of thumb. Academic press; 2014.

[44] Baster ME. Modelling the performance of Air Source Heat Pump Systems. 2011.

[45] Kirnak H, Hansen RC, Keener HM, Short TH. An evaluation of physically based and empirically determined evapotranspiration models for nursery plants. Turkish J Agric For 2002;26:355–62. https://doi.org/10.3906/tar-0112-4.

[46] Pamungkas AP, Hatou K, Morimoto T. Evapotranspiration Model Analysis of Crop Water Use in Plant Factory System. Environ Control Biol 2014;52:183–8. https://doi.org/10.2525/ecb.52.183.

[47] Stanghellini C. Transpiration of Greenhouse Crops. Wageningen University, 1987.

[48] Massmann A, Gentine P, Lin C. When Does Vapor Pressure Deficit Drive or Reduce Evapotranspiration? J Adv Model Earth Syst 2019;11:3305–20. https://doi.org/10.1029/2019MS001790.

[49] Proietti S, Moscatello S, Leccese A, Colla G, Battistelli A. The effect of growing spinach (Spinacia oleracea L.) at two light intensities on the amounts of oxalate, ascorbate and nitrate in their leaves. J Hortic Sci Biotechnol 2004;79:606–9. https://doi.org/10.1080/14620316.2004.11511814.

[50] Qaddoum K, Hines EL, Iliescu DD. Yield Prediction for Tomato Greenhouse Using EFuNN. ISRN Artif Intell 2013;2013:1–9. https://doi.org/10.1155/2013/430986.

[51] Erwin J, Gesick E. Photosynthetic responses of swiss chard, kale, and spinach cultivars to irradiance and carbon dioxide concentration. HortScience 2017;52:706–12. https://doi.org/10.21273/HORTSCI11799-17.

[52] Shao Y, Heath T, Thu Y. Developing an economic estimation system for vertical farms. Int J Agric Environ Inf Syst 2016;7.

[53] Schnitzler WH, Sharma AK, Gruda NS, Heuberger HT. A low-tech hydroponic system for bell pepper (capsicum annuum L.) production. Acta Hortic., vol. 644, International Society for Horticultural Science; 2004, p. 47–53. https://doi.org/10.17660/ActaHortic.2004.644.3.

[54] Benis K, Reinhart C, Ferrão P. Development of a simulation-based decision support workflow for the implementation of Building-Integrated Agriculture (BIA) in urban contexts. J Clean Prod 2017;147:589–602. https://doi.org/10.1016/j.jclepro.2017.01.130.

[55] Vanthoor BHE, de Visser PHB, Stanghellini C, van Henten EJ. A methodology for model-based greenhouse design: Part 2, description and validation of a tomato yield model. Biosyst Eng 2011;110:378–95. https://doi.org/10.1016/j.biosystemseng.2011.08.005.

[56] Gómez C, Izzo LG. Increasing efficiency of crop production with LEDs. AIMS Agric Food 2018;3:135–53. https://doi.org/10.3934/agrfood.2018.2.135.

[57] Benis K, Reinhart C, Ferrão P. Building-Integrated Agriculture (BIA) In Urban Contexts : Testing A Simulation-Based Decision Support Workflow. 15th IBPSA Conf. San, 2017.

[58] Pan T, Wang Y, Wang L, Ding J, Cao Y, Qin G, et al. Increased CO2 and light intensity regulate growth and leaf gas exchange in tomato. Physiol Plant 2020;168:694–708. https://doi.org/10.1111/ppl.13015.

[59] Iddio E, Wang L, Thomas Y, McMorrow G, Denzer A. Energy efficient operation and modeling for greenhouses: A literature review. Renew Sustain Energy Rev 2020;117:109480. https://doi.org/10.1016/j.rser.2019.109480.

[60] Pieters JG, Deltour JM. Performances of greenhouses with the presence of condensation on cladding materials. J Agric Eng Res 1997;68:125–37. https://doi.org/10.1006/jaer.1997.0187.

[61] Shen Y, Wei R, Xu L. Energy consumption prediction of a greenhouse and optimization of daily average temperature. Energies 2018;11. https://doi.org/10.3390/en11010065.

[62] iFarm. How Much Electricity Does a Vertical Farm Consume Using iFarm technologies? n.d. https://ifarm.fi/blog/2020/12/how-much-electricity-does-a-vertical-farm-consume (accessed March 26, 2021).

[63] Harbick K, Albright LD. Comparison of energy consumption: Greenhouses and plant factories. Acta Hortic 2016;1134:285–92. https://doi.org/10.17660/ActaHortic.2016.1134.38.

[64] Kempkes FLK, Janse J. Cultivation and energy 2SaveEnergy greenhouse 2016.

[65] Castleton HF, Stovin V, Beck SBM, Davison JB. Green roofs; Building energy savings and the potential for retrofit. Energy Build 2010;42:1582–91. https://doi.org/10.1016/j.enbuild.2010.05.004.

[66] Shin HH, Nam SW. Validation of load calculation method for greenhouse heating design and analysis of the influence of infiltration loss and ground heat exchange. Korean J Hortic Sci Technol 2015;33:647–57. https://doi.org/10.7235/hort.2015.15007.

[67] Shamshiri RR, Jones JW, Thorp KR, Ahmad D, Man HC, Taheri S. Review of optimum temperature, humidity, and vapour pressure deficit for microclimate evaluation and control in greenhouse cultivation of tomato: A review. Int Agrophysics 2018;32:287–302. https://doi.org/10.1515/intag-2017-0005.